

The local sub-mm luminosity functions and predictions from Spitzer to Herschel

Stephen Serjeant¹ and Diana Harrison^{2,3}

¹ *Centre for Astrophysics and Planetary Science, School of Physical Sciences, University of Kent, Canterbury, Kent, CT2 7NZ, UK*

² *Astrophysics Group, Blackett Laboratory, Imperial College, Prince Consort Road, London SW7 2BW, UK*

³ *Dept. of Physics, Cavendish Laboratory, Madingley Road, Cambridge CB3 0HE, UK*

Accepted; Received; in original form 2003 March 4

ABSTRACT

We present new determinations of the local sub-mm luminosity functions, solving the “sub-mm Olbers’ Paradox.” We also present predictions of source counts and luminosity functions in current and future far-infrared to sub-mm surveys. Using the sub-mm colour temperature relations from the SCUBA Local Universe Galaxy Survey, and the discovery of excess $450\mu\text{m}$ excess emission in these galaxies, we interpolate and extrapolate the IRAS detections to make predictions of the SEDs of all 15411 PSC-z galaxies from $50 - 1300\mu\text{m}$. Despite the long extrapolations we find excellent agreement with (a) the $90\mu\text{m}$ luminosity function of Serjeant et al. (2001), (b) the $850\mu\text{m}$ luminosity function of Dunne et al. (2000), (c) the mm-wave photometry of Andreani & Franceschini (1996); (d) the asymptotic differential and integral source count predictions at $50 - 1300\mu\text{m}$ by Rowan-Robinson (2001). We find the local $850\mu\text{m}$ sub-mm luminosity density converges to $7.3 \pm 0.2 \times 10^{19} h_{65} \text{ W Hz}^{-1} \text{ Mpc}^{-3}$. Remarkably, the local spectral luminosity density and the extragalactic background light together strongly constrain the cosmic star formation history for a wide class of evolutionary assumptions. We find that the extragalactic background light, the $850\mu\text{m}$ 8mJy source counts, and the Ω_* constraints all independently point to a decline in the comoving star formation rate at $z > 1$. In order to reconcile this with direct determinations, we suggest either there is a top-heavy initial mass function at high redshifts, and/or there is stronger evolution in the more luminous far-infrared galaxies than seen in the population as a whole.

Key words: cosmology: observations - galaxies: formation - infrared: galaxies - galaxies: evolution - galaxies: starburst - galaxies: statistics

1 INTRODUCTION

The high expectations for sub-mm/mm-wave surveys have been fully and variously realised. The discovery of a population of $z > 1$ sub-mm galaxies resolving up to 50% of the extragalactic background light, and the surprising lack of overlap with the hard X-ray Chandra populations, have been among the key results in cosmology of the past five years. The SCUBA survey of the Hubble Deep Field (HDF) demonstrated the feasibility of blank-field surveys (Hughes, Serjeant, Dunlop, Rowan-Robinson, et al. 1998, Serjeant et

al. 2003), and several complementary sub-mm/mm-wave surveys have since been conducted to a variety of depths and areal coverages (e.g. Scott et al. 2002; Fox et al. 2002; Eales et al. 2000; Barger et al. 1999). These surveys will be augmented with much larger surveys with (e.g.) SCUBA-2 (e.g. Holland et al. 2002), BOLOCAM on the CSO (e.g. Glenn et al. 1998), the Balloon-borne Large Aperture Sub-mm Telescope (e.g. Tucker et al. 2004), the Large Millimeter Telescope (e.g. Kaercher et al. 2000), the Atacama Large Millimeter Array (ALMA), Planck High Fre-

quency Instrument (HFI, e.g. Lamarre et al. 2001), and Herschel SPIRE (e.g. Griffin et al. 2001).

It is not widely appreciated that the most reasonable prior expectation for the SCUBA-HDF survey, based on the observed optical HDF population, was *zero* sources at $850\mu\text{m}$: for example, Thompson et al. (2001) model the near-IR/optical/near-UV SEDs of the NICMOS-HDF galaxies, and derive sub-mJy/*micro*-Jy fluxes at $850\mu\text{m}$. The mJy-level sub-mm galaxies found in blank-field surveys on the whole can be reasonably regarded as a new galaxy population.

One attractive interpretation of this new population is that it is comprised at least in part of proto-spheroids (e.g. Dunlop 2001): the star formation rates inferred in sub-mm survey galaxies ($\gtrsim 1000 M_{\odot}/\text{yr}$) are sufficient to assemble a giant elliptical galaxy in $< 1\text{Gyr}$. In support of this interpretation, the K-band morphologies of at least some resemble high-redshift radiogalaxies (Lutz et al. 2002), and provisional measurements of the clustering are consistent with a high bias parameter population at high redshift (Scott et al. 2002). Nevertheless, the sub-mm galaxies are not unambiguously identified with proto-spheroids; Rowan-Robinson (2001), Efstathiou & Rowan-Robinson (2002) and King & Rowan-Robinson (2003) instead postulate that the blank-field sub-mm survey galaxies are dominated in the sub-mm by cirrus heated by their interstellar radiation fields, rather than ultraluminous star formation. In support of this interpretation, Efstathiou & Rowan-Robinson (2002) model the SEDs of sub-mm galaxies and find them consistent with their cirrus radiative transfer models. The existence of cool colour temperature components in local galaxies, physically distinct from the warmer dust dominating the $60\mu\text{m}$ emission, have been pointed out by many authors (e.g. Dunne et al. 2000 and refs. therein, Stickel et al. 2000, Siebenmorgen et al. 1999, Domingue et al. 1999, Trewhella et al. 2000; Haas et al. 2000.) If this cool component dominates the observed sub-mm fluxes of high- z blank field sub-mm/mm-wave survey sources, then the emission should be extended over $\sim 1''$ rather than confined to a compact $\sim 0.1''$ ultraluminous starburst (Efstathiou & Rowan-Robinson 2002, Lee & Rowan-Robinson 2003, Kaviani et al. 2002). This distinction will be possible with the planned ALMA.

In the meantime, the evolution of the sub-mm galaxy population can be strongly constrained by the integrated extragalactic background light, the local multiwavelength luminosity functions, and the source counts. The local $850\mu\text{m}$ luminosity function was derived in the SCUBA Local Universe Galaxy Survey (SLUGS, Dunne et al. 2000) from their SCUBA photometry of the IRAS Bright Galaxy Survey. A curious aspect of their luminosity function was that the faint end slope was not sufficiently shallow for the local luminosity density to converge, which the authors re-

ferred to as the “sub-mm Olbers’ paradox”. This is a pity from the point of view of modelling the high redshift population, since the integrated extragalactic background light is a key constraint. In order to find the expected flattening of the luminosity function slope at lower luminosities, the SLUGS survey is currently being extended with SCUBA photometry of optically-selected galaxies. Meanwhile, several authors have attempted to use the colour temperature – luminosity relation found in SLUGS to transform the $60\mu\text{m}$ luminosity function to other wavelengths, and hence constrain the high-redshift evolution (e.g. Lagache, Dole & Puget 2003, Lee & Rowan-Robinson 2003, Chapman et al. 2003). The discovery of an additional excess component at $450\mu\text{m}$ (Dunne & Eales 2001) relative to their initial colour temperature – luminosity relation is only rarely included in such models (e.g. Lagache, Dole & Puget 2003), and there are problems in accurately representing the population mix of galaxies.

In this paper we take an alternative approach to determining the multiwavelength local luminosity functions. We model the spectral energy distributions (SEDs) of all 15411 PSC- z galaxies (Saunders et al. 2000), constrained by all available far-infrared and sub-mm colour-colour relations from SLUGS and elsewhere. This guarantees the correct local population mix at every wavelength and minimises the assumptions about the trends of SED shape with luminosity (see e.g. Rowan-Robinson et al. 2001, in which the differences in assumed population mix result in rather different conclusions to this work). Our phenomenological approach is sufficient to determine (for example) the $850\mu\text{m}$ luminosities to within a factor of 2 in individual galaxies. While this is not accurate enough to serve as calibrations for sub-mm missions, except statistically over the whole population, it is more than sufficiently accurate for determining local luminosity functions, which we present here from far-infrared to millimetric wavelengths. We use these local luminosity functions to model the high- z evolution, constrained by the extragalactic background light spectrum, the total cosmological matter density in stars Ω_* , and the sub-mm source counts.

Our SED models are accurate enough to identify potential calibrators for further photometric study. The SEDs can also be used to determine the bright source contributions to current and future far-infrared and sub-mm/mm-wave surveys. Predictions for bright source catalogues are also essential tools for the planning and execution of future wide area far-infrared missions. For example, the catalogues are useful for both tertiary flux calibration and astrometric calibration in all-sky surveys (e.g. Planck HFI, Astro-F, e.g. Pearson et al. 2001, Shibai 2002), and also for mission strategy (such as deep survey fields avoiding bright sources).

Section 2 describes our modelling of the spectral energy distributions, including observational tests of

our methodology. Section 3 presents the results, such as multiwavelength local luminosity functions, and bright source counts for Planck HFI, Herschel SPIRE, and Astro-F. The implications of our results are discussed in section 4.

Throughout this paper we adopt the “concordance” cosmology of $\Omega_M = 0.3$, $\Omega_\Lambda = 0.7$ and $H_0 = 65 \text{ km s}^{-1} \text{ Mpc}^{-1}$.

2 METHOD

2.1 850 μm predictions

The PSC-z survey is a redshift survey of IRAS galaxies, to a depth of 0.6Jy at 60 μm . PSC-z covers 84% of the sky, and has a median redshift of 8400 km s^{-1} . Further details can be found in Saunders et al. (2000).

Our first stage in modelling the far-infrared to mm-wave SEDs of IRAS PSC-Z galaxies is to determine their 850 μm fluxes. To do this we use the results from the 850 μm photometry programme of the IRAS Bright Galaxy Sample by Dunne et al. (2000). These authors found a strong correlation between far-infrared luminosity and sub-mm:far-infrared colour. The far-infrared luminosity correlates strongly with the 60 – 100 μm colour, so an alternative approach to modelling the luminosity-colour relation is to fit to the 100 – 60 μm vs. 850 – 60 μm colour-colour plane. This is plotted in figure 1, together with the predictions from grey-body emission:

$$S_\nu = \nu^\beta B_\nu = \nu^\beta \frac{2h\nu^3}{c^2} \frac{1}{\exp(h\nu/(kT)) - 1} \quad (1)$$

The lines in figure 1 correspond to $\beta = 1.1, 1.2, 1.3, 1.4, 1.5$. Dunne et al. (2000) also modelled the colour temperatures and β values for all their sample using limited 450 μm data, and found a median $\beta = 1.3$ which is in excellent agreement with the best fit to figure 1. Physically, these galaxies are very unlikely to be single temperature or even dual temperature systems (e.g. Efstathiou, Rowan-Robinson & Siebenmorgen 2000) but all that matters for our current purpose is that we have a phenomenological model which can be used to interpolate to other frequencies.

We use the co-added or extended ADDSCAN IRAS fluxes (Saunders et al. 2000). For the 29% of sources with only 100 μm limits, we use the non-linear 60 μm -100 μm luminosity-luminosity correlation (i.e., the well-known trend of IRAS colour temperature correlating with luminosity) to estimate the 100 μm fluxes. Redshift information is available for almost all of PSC-Z, but because redshift is degenerate with colour temperature this information is not necessary for sub-mm flux prediction where 100 μm detections are available.

Figure 1. Sub-mm:far-infrared colour-colour plane for the Dunne et al. (2000) sample. From top to bottom, lines show the predictions for grey body indices of $\beta = 1.1, 1.2, 1.3, 1.4, 1.5$.

2.2 450 μm predictions and interpolations/extrapolations

While the phenomenological model above is a good predictor of the 850 μm fluxes of IRAS galaxies, there is an additional component at shorter wavelengths discovered by Dunne & Eales (2001).

The combined 850 μm , 450 μm , 100 μm and 60 μm data of the IRAS Bright Galaxy Survey led Dunne & Eales (2001) to argue for two $\beta = 2$ grey-body components, because the excess flux in the short-wavelength sub-mm data could not be fit by any single grey-body template. As the two component model is a four-parameter fit (two temperatures and two normalisations) with the emissivity fixed, four-band photometry is just sufficient in principle to define the fit uniquely.

Together with the IRAS measurements, our prescription for 850 μm fluxes gives us a total of three bands on which to base SED interpolations. We can obtain a further phenomenological prediction for the 450 μm fluxes on the linear 60 : 850 μm vs. 60 : 450 μm colour-colour correlation, for which the IRAS Bright Galaxy Survey yields

$$\log_{10}(S_{60}/S_{450}) = \log_{10}(S_{60}/S_{850}) - 0.924 \quad (2)$$

These prescriptions should be sufficient to define the sub-mm fluxes to within a factor of two.

We then numerically solve for the parameters of the two temperature components, using the four-band measured and predicted photometry. Note that this two component fit uses a grey body index of $\beta = 2$, which is not consistent with the $\beta = 1.3$ model used to predict the 850 μm fluxes. This does not affect the

self-consistency or utility of the two-component fit, because the only relevant information is that a numerical scheme of whatever nature is available to predict the $850\mu\text{m}$ fluxes of the IRAS PSC-Z galaxies. Also, it is worth stressing again that more physically reasonable models incorporate a continuum of temperature components; all that matters for our current purpose is to obtain a phenomenological parametric model on which to base predictions of the far-IR to mm-wave SEDs. In the following section we will test the consistency of the phenomenological predictions using a variety of observational constraints.

The dual-temperature model incorporates the available photometric constraints on the far-infrared to mm-wave SEDs of IR-luminous galaxies, and provides the best available interpolations and extrapolations from $50 - 1300\mu\text{m}$ in an all-sky catalogue. The PSC-Z predictions for Astro-F, Herschel, Planck HFI and ISO are available as an IDL database from the authors. Also available is interpolation software to provide further predictions at further arbitrary wavelengths.

3 RESULTS

3.1 Observational tests

In figure 2 we plot the observed 1.25mm photometry of Andreani & Franceschini (1996), compared with our predictions. These observations are subject to a systematic uncertainty of up to a factor of 2 due to aperture corrections. Notwithstanding a large systematic shift in flux calibration, our predictions are in good agreement with these observations.

A stronger tests of our methodology comes from the Serendipity Survey of the Infrared Space Observatory (ISOSS), taken at $175\mu\text{m}$ by the ISOPHOT instrument (e.g. Stickel et al. 2000). The survey covered $\sim 10\%$ of the sky, and although the completeness is not yet well understood the flux calibration is well-determined enough to provide a useful test. Figure 3 shows the predicted $175\mu\text{m}$ fluxes against those observed. The agreement is excellent. This also demonstrates that the cool dust excess reported by Stickel et al. (2000) is identical to that reported by Dunne & Eales (2001), at least insofar as fitting of SEDs with colour temperature components is concerned. (This does not necessarily imply the $175\mu\text{m}$ -emitting dust is copatial to the $450\mu\text{m}$ -emitting dust, e.g. section 3.3.)

There are few other examples of objects with sufficient multi-wavelength coverage to provide tests of our methodology (a problem also encountered by other authors: e.g. Hughes et al. 2002). In figure 4 we plot the ratio of our predictions with the observations for the SLUGS survey, as a function of wavelength. The dispersion is a measure of the error in our predictions for individual objects, while the mean values demonstrate that the systematic errors in our

Figure 2. Comparison of predicted and observed 1.25mm fluxes for the sample of Andreani & Franceschini 1996, using their $\alpha_{\text{mm}} = \alpha_{\text{o}}/3$ aperture correction. Their alternative $\alpha_{\text{mm}} = \alpha_{\text{o}}$ aperture corrections result in an upward revision of the observed fluxes by a factor of $\sim \times 1.5 - 2$. The straight line indicates the locus of exact agreement between observations and predictions.

methodology are typically only at the few percent level in the wavelength range covered. Our systematic agreement is slightly better than that of Dale et al. (2001, 2002) who use a single-component SED but with a varying grey body index.

One of the individual galaxies in the SLUGS survey, also covered by the ISOSS survey, is shown in figure 5. The agreement is again very good. Note that this is *not* a fit to the multi-wavelength data; instead, the model is the mean SED for a galaxy with the $60 : 100\mu\text{m}$ colour of this galaxy.

3.2 Multi-wavelength local luminosity functions

Our sample is $60\mu\text{m}$ -selected, but that does not preclude us from constructing a luminosity function at another wavelength provided there are no large populations that would be missing from our sample at *any* redshift, compared to a flux limited sample at that other wavelength. Serjeant et al. (2001) describe the methodology for deriving luminosity functions in the face of complicated selection functions, and the conditions for the validity of such derivations. In summary,

Figure 3. Comparison of predicted and observed $175\mu\text{m}$ fluxes for the ISOPHOT Serendipity Survey of Stickel et al. (2000), using the best available current flux calibration (Stickel. priv. comm.).

the number density in a given luminosity bin is given by

$$\Phi = \Sigma(V_{\text{max},i})^{-1} \quad (3)$$

and the error on this quantity is given by

$$\Delta\Phi = \sqrt{\Sigma(V_{\text{max},i})^{-2}} \quad (4)$$

Here, $V_{\text{max},i} = V(z_{\text{max},i})$ where V is the comoving volume, and $z_{\text{max},i}$ is the redshift at which object i would be observed at the $60\mu\text{m}$ PSC-z flux limit, if all other intrinsic properties of that object were kept the same. Our methodology differs slightly from that of Takeuchi et al. (2003), in that those authors used different K-corrections and a different sub-samples (warm and cool) of the PSC-z survey, as well as making a correction for density fluctuations. These differences in methodology lead to small changes in (for example) the faint end slope, but are too small to affect the conclusions of our paper.

Although we have found that the $850\mu\text{m}$ predictions for individual galaxies are only good to within a factor of ~ 2 (figure 4), this is nevertheless accurate enough for the determination of the local luminosity function. Note that these luminosities are estimated directly from the colour-colour relations, and are not interpolated using our two-component dust models (except for the K-correction terms). In fig-

Figure 4. Comparison of the observed SEDs of SLUGS galaxies with the predictions of this paper. The \times symbols indicate the SLUGS measurements themselves, while the $+$ symbols represent the supplementary data compiled from the literature by Dunne & Eales (2001).

ure 6, we plot the $1/V_{\text{max}}$ $850\mu\text{m}$ luminosity function for PSC-Z assuming $(1+z)^3$ pure luminosity evolution (an assumption which makes a small correction to only the brightest data points), and compare it to the observed luminosity function from Dunne et al. (2000). The agreement is excellent, and as with further multi-wavelength luminosity functions below is sufficient to determine the convergence of the local luminosity density. This is shown in the case of the $850\mu\text{m}$ luminosity density in figure 7, where the PSC-z constraints are compared to the existing SLUGS data. The SLUGS data reaches the peak of the luminosity density, but would need to extend around $\sim \times 10$ fainter to determine the convergence in the background. Using PSC-z, we find that local luminosity density at $850\mu\text{m}$ converges at $7.3 \pm 0.2 \times 10^{19} h_{65} \text{ W Hz}^{-1} \text{ Mpc}^{-3}$, solving the sub-mm Olbers' Paradox. The constraints at other wavelengths will be discussed in further detail in section 3.3.

Unlike the $850\mu\text{m}$ luminosity function, the $90\mu\text{m}$ luminosities do not have direct colour-colour relations to use for their prediction. We therefore resort to the two-component SEDs to derive interpolated $90\mu\text{m}$ fluxes. In figure 8 we plot the predicted $90\mu\text{m}$ luminosity function for PSC-Z, and compare it to the observed luminosity function from the European Large

Figure 12. Continuation of figure 11.

λ (μm)	$\log_{10} \Phi_{*,S}$ ($\text{dex}^{-1} \text{ Mpc}^{-3}$)	$\log_{10} L_{*,S}$ ($\text{W Hz}^{-1} \text{ sr}^{-1}$)	α	$\log_{10} \Phi_{*,P}$ ($\text{dex}^{-1} \text{ Mpc}^{-3}$)	$\log_{10} L_{*,P}$ ($\text{W Hz}^{-1} \text{ sr}^{-1}$)	β	γ
70	-3.72	23.69	1.73	-3.27	23.56	0.705	3.04
90	-3.43	23.69	1.63	-2.93	23.54	0.567	2.84
160	-3.09	23.55	1.50	-2.91	23.61	0.558	3.47
175	-3.08	23.51	1.50	-2.93	23.58	0.583	3.56
250	-2.98	23.19	1.43	-2.78	23.23	0.481	3.28
350	-2.93	22.80	1.39	-2.92	22.96	0.536	4.28
450	-2.92	22.48	1.38	-2.73	22.53	0.446	3.30
500	-2.88	22.31	1.35	-2.70	22.36	0.415	3.29
550	-2.91	22.19	1.38	-2.74	22.25	0.456	3.35
850	-2.90	21.54	1.38	-2.73	21.61	0.458	3.36

Table 1. Best-fit parameters for the luminosity functions shown in figure 9. The parameters are defined in equations 5 and 6.

Figure 5. Comparison of the observed SED of NGC520 with the predictions. The cool and warm components are shown separately, and the sum (also shown) is in good agreement with the observations. References for the photometry are in Dunne & Eales (2001).

Area ISO Survey (Serjeant et al. 2001). Pure luminosity evolution of $(1+z)^3$ was assumed.

The $175\mu\text{m}$ luminosity function cannot be determined directly from the ISOSS survey, because the completeness of this survey is not well-understood. In figure 9 we plot the predicted $175\mu\text{m}$ luminosity function from our PSCZ models, and further examples of the interpolated luminosity functions possible from our PSC-z SED ensemble. The $175\mu\text{m}$ luminosity function is currently the best constraint available at around this wavelength before Spitzer and Astro-F,

Figure 6. Projected local $850\mu\text{m}$ luminosity function from PSC-Z (error bars) assuming pure luminosity evolution of $(1+z)^3$, compared with the directly measured luminosity function from Dunne et al. 2000 (plotted as open circles). Also plotted are the best fit Schechter and double power law functions (dashed and dotted lines respectively).

because the number of local $175\mu\text{m}$ -selected galaxies from the European Large Area ISO Survey (Oliver et al. 2000) and FIRBACK (Dole et al. 2001) is too small for the construction of a luminosity function.

Table 1 shows the min- χ^2 fit parameters for the local luminosity functions discussed in this section, using the following functional forms:

$$\Phi = \Phi_{*,S} \ln(10) (L/L_{*,S})^{1-\alpha} e^{-L/L_{*,S}} \quad (5)$$

$$\Phi = \Phi_{*,P} / ((L/L_{*,P})^\beta + (L/L_{*,P})^\gamma) \quad (6)$$

Figure 7. Projected local $850\mu\text{m}$ luminosity density function from PSC-Z (error bars), compared with the directly measured luminosity density from Dunne et al. 2000 (plotted as open circles). This is derived directly from figure 6 after removal of the sr^{-1} factor in the luminosities. Note that the addition of the PSC-z data adds the first evidence of convergence in the local luminosity density at $850\mu\text{m}$.

The Schechter functions give acceptable χ^2 values when restricted to data less than a few times L_* , but in no cases provide an acceptable fit at the brightest end. The double power law fit, on the other hand, fits all the available data.

3.3 The local extragalactic luminosity density

The extraordinarily tight constraints on the far-infrared to sub-mm luminosity functions in section 3.2 allow us to make tight constraints on the local extragalactic spectral luminosity density. This is plotted in figure 10. The vertical lines indicate where direct constraints on the PSC-z luminosity densities are available via IRAS, SCUBA or ISO. These are spaced roughly in factors of 2 in wavelength. Between these wavelengths, the luminosity densities are based on interpolated flux densities using our two-component SED models. The thickness of the line is the $\pm 1\sigma$ error on the luminosity density.

Remarkably, the local spectral luminosity density itself can be described to within better than a percent by two grey bodies, despite being comprised of the

Figure 8. Projected local $90\mu\text{m}$ luminosity function from PSC-Z (error bars), compared with the directly measured luminosity function from ELAIS (shaded area) from Serjeant et al. 2001. In both cases pure luminosity evolution of $(1+z)^3$ was assumed. Also plotted are the best fit Schechter and double power law functions (dashed and dotted lines respectively).

sum of > 30000 individual grey bodies:

$$I_\nu(0)(\text{WHz}^{-1}\text{Mpc}^{-3}) = \frac{5.93 \times 10^{34}}{\lambda^{5.03}(\exp(705.4/\lambda) - 1)} + \frac{3.87 \times 10^{31}}{\lambda^{4.50}(\exp(318.0/\lambda) - 1)} \quad (7)$$

where λ is in μm , and I is in W/Hz/Mpc^3 . This is an instructive lesson: one should not use the two components of our model (or that of Dunne & Eales 2001) to argue for two discrete, physically distinct phases. The two components are a simple phenomenological model, and do not preclude a continuum of dust temperatures being present. It is also easy to demonstrate that the results of radiative transfer models of star forming regions (e.g. Efstathiou et al. 2000) can often be fit to within a few percent by a small number of grey bodies, even though a continuum of temperatures is intrinsic to the models.

Finally, one can use equation 7 to calculate the local bolometric luminosity density from thermal dust emission. In the interval $30\mu\text{m}$ - 3mm , this is found to be $2.6 \times 10^{34} \text{ W Mpc}^{-3}$, i.e. $6.4 \times 10^7 L_\odot \text{ Mpc}^{-3}$, in very good agreement with the determination by Dwek et al. 1998. (Differences in the SED ensemble

Wavelength (μm)	k ($\text{Jy}^{1.5} \text{sr}^{-1}$)
70	1642
90	2858
160	3146
175	2848
250	1166
350	347
450	116
500	71.3
550	45.2
850	4.92

Table 2. Approximate asymptotic Euclidean source count slopes for the predicted source counts plotted in figure 11. These asymptotic counts follow $dN/dS = kS^{-2.5}$, with the coefficient k listed in the table as a function of wavelength.

3.4 Bright source counts from Astro-F to Herschel

Figures 11 and 12 show the bright source counts at wavelengths covered by Spitzer, Astro-F, BLAST (Tucker et al. 2004), SCUBA, MAMBO, Herschel, and Planck. The bright slopes are Euclidean as expected (table 2), but at faint fluxes the counts fall below the Euclidean extrapolation. This is an incompleteness due to the $60\mu\text{m}$ flux limit of PSC-z: of the local galaxies at the faint end of the sub-mm counts, only the warmer will appear in a $60\mu\text{m}$ -limited survey. It is possible to correct for this using accessible-volume weightings. This is essentially equivalent to constructing luminosity functions, discussed above, but the resulting statistic (confirmation of Euclidean slope) would have less utility and interest than the luminosity functions themselves. Furthermore, PSC-z is not deep enough to detect the sub-mm blank-field survey population, both because of the less favourable K-corrections and because of the low median redshift of PSC-z itself. Therefore, deviations from the Euclidean slope caused by high-z evolution will not be well-determined by PSC-z.

How similar are our PSC-Z “simulated” catalogues at each wavelength to flux-limited surveys at those wavelengths? There are two types of object which could be undetected by IRAS: local galaxies too faint in the IRAS bands due to their intrinsic luminosities and colour temperatures, and high-redshift galaxies beyond the upper redshift limit of PSC-Z. An indication of the fluxes at which local galaxies start to be missed is the point at which the counts depart from the Euclidean slope, in figures 11 and 12. Note that this is not an effect which would alter the luminosity functions, provided there are no populations which would be missing at *any* redshift. On the other hand, the level at which high-z populations are seen depends strongly on the assumed evolution of these galaxies. As an indication of the level of this effect,

Figure 10. Local spectral luminosity density. The thickness of the curve represents the $\pm 1\sigma$ error. Vertical lines indicate the wavelengths where direct estimates are available from colour-colour relations using PSC-Z, or wavelengths where direct observational tests verify the methodology. The values of the local luminosity density at intervening wavelengths use the two component dust models of PSC-z.

do however generate differences in our local spectral luminosity density, compared to that of Dwek et al. 1998.) The SED models however are not constrained over all this range; the local luminosity density over the range $60 - 1300\mu\text{m}$ is $5.3 \times 10^7 L_{\odot} \text{Mpc}^{-3}$. Our local bolometric luminosity density differs from that of Soifer and Neugebauer (1991) owing to the different bolometric corrections for each galaxy, but our integrated luminosity density over the range $50 - 100\mu\text{m}$ (i.e. the overlap range in measurements and model validity) is in good agreement: $4.9 \times 10^6 L_{\odot} \text{Mpc}^{-3}$, compared to the result of integrating the Soifer & Neugebauer data over this range to obtain $6.3 \times 10^6 L_{\odot} \text{Mpc}^{-3}$. The integrated background in the *optical* is much larger: $1.26 \times 10^8 L_{\odot} \text{Mpc}^{-3}$ (Glazebrook et al. 2003). The fact that the extragalactic background has a larger luminous energy fraction in the far-infrared implies stronger relative evolution in the far-infrared luminous population (e.g. Puget et al. 1996, Hauser et al. 1998, Schlegel et al. 1998, Rowan-Robinson 2001, Smail et al. 2002).

we overplot predictions from the source count model of Rowan-Robinson (2001). The slight deviations of the model from the Euclidean slope is thought to be a numerical artifact (Rowan-Robinson priv. comm.).

3.5 High-redshift evolution

Can we use our local luminosity functions (section 3.2) and the local spectral luminosity density (section 3.3) to constrain the cosmic star formation history? An exhaustive analysis of the constraints is beyond the scope of this paper; however, we note here that the extragalactic background light is determined entirely by the evolving spectral luminosity density:

$$I_\nu(\nu) = \frac{1}{4\pi} \int_0^\infty j_\nu(\nu', z) \frac{R_0 dr}{(1+z)} \quad (8)$$

where j_ν is the comoving spectral luminosity density, and $R_0 dr$ the comoving distance element (Peacock 2001; see also Hauser & Dwek 2001). A very large class of evolutionary models including pure luminosity, pure density, and mixed luminosity/density, satisfy

$$j_\nu(z) = j_\nu(z=0)f(z) \quad (9)$$

where $f(z)$ is the Madau diagram normalised to 1 at $z=0$. We assume the far-infrared luminosity density is proportional to the volume-average star formation rate, following Rowan-Robinson 2001 (see equation 11 below). A further assumption which underpins this, and indeed almost every study of the high- z sub-mm population, is that local galaxies can be found which are reliable templates of the high- z population. This is not necessarily the case, in which case equation 9 will not hold. Nevertheless, if local galaxies *are* reliable templates, equation 9 will hold in very general conditions.

We can therefore use the observed extragalactic background light spectrum to constrain the dust-enshrouded cosmic star formation history, *independently* of constraints from redshift surveys of sub-mm blank-field surveys. This has been attempted by other authors (e.g. Gispert et al. 2000, Dwek et al. 1998) but without the benefit of a robust determination of the local luminosity density $I_\nu(z=0)$. The authors therefore had to resort to assuming a small number of template SEDs, and explore the parameter space of $f(z)$ allowed by range of SED models. We have the benefit of a very well-constrained determination of $I_\nu(z=0)$.

The determinations of the far-infrared extragalactic background light historically have fluctuated in the literature, mainly reflecting the discovery and differing treatment of systematics (e.g. Puget et al. 1996, Fixsen et al. 1998). We adopt the determination of Lagache et al. (1999), since this is corroborated by separate analysis of low-cirrus fields, and by the decomposition using the WHAM H α survey and Leiden/Dwingeloo HI data (Lagache et al. 2000). We

Figure 15. Example of the $\pm 1\sigma$ constraints on the cosmic star formation history defined in figure 13. Models are plotted which satisfy both the sub-mm source counts constrain and the $\pm 1\sigma$ likelihood range based on our analysis of the extragalactic background light. Note that the value of the peak redshift z_t is *strongly* correlated with that of the evolution rate A , in that high values of z_t require lower values of A , as can also clearly be seen in figure 13. Section 4 discusses how these constraints be resolved with direct determinations.

do not fit to DIRBE data shortward of $200\mu\text{m}$, since these predictions rely mainly on an *extrapolation* of our SEDs in their rest-frames rather than an *interpolation*. Warmer dust components are inevitable, regardless of starburst or AGN activity, but are not incorporated into our SED models. We defer treatment of these warmer components, their associated colour-colour diagrams, and of the DIRBE points, to a later paper.

We found that the extragalactic background light can be fit by a sequence of judiciously-placed δ -functions in $f(z)$, and that there is no unique choice for these δ -functions. Therefore, a unique deconvolution of $f(z)$ from the extragalactic background light is not possible within the observational errors in the background. However, we can still make useful constraints if we restrict the class of allowed forms for $f(z)$. For simplicity, and to demonstrate the types of

Figure 14. Left figure shows the extragalactic background light (data from Lagache et al. 1999) modelled by the cosmic star formation history in equation 10. The data longward of $200\mu\text{m}$ plotted as broken lines is the FIRAS spectrum: full line is whole sky, and dashed line is Lockman Hole only. Also plotted are the DIRBE data points, not included in our fitting. The smooth curves are models of this spectrum, corresponding to cosmic star formation histories plotted in the right hand figure, *provided our assumption about the evolving luminosity density (equation 9) holds*. The full line is the global maximum likelihood fit quoted in table 3, and the long-dashed line has the same parameters except an enhanced high- z star formation rate ($B = 0.25$) which is marginally ($\sim 2\sigma$) inconsistent with the extragalactic background. The two short-dashed lines demonstrate selected alternative models: $z_t = 1$ and $z_t = 2$, both with $A = 3$ and $B = 1$. Note that in general the models with the higher star formation rates at $z > 2$ are also the models predicting the larger background at wavelengths $\lambda \sim 1\text{mm}$ (including in particular a comparison of the two short-dashed curves). In general, models with high volume-averaged star formation rates at $z > 2$ overpredict the sub-mm/mm-wave background.

constraints which are available on f , we model the Madau diagram $f(z)$ with the following simple parameterisation:

$$f(z) = (1+z)^A \quad [z < z_t] \quad (10)$$

$$f(z) = (1+z_t)^A B^{z-z_t} \quad [z \geq z_t]$$

i.e., $(1+z)^A$ power-law evolution to a threshold redshift z_t , and an arbitrary decline thereafter which we have chosen to be a straight line in the $\log f - z$ plane.

The results of this fitting are shown in figure 13, where we plot the confidence limits on A and z_t marginalised over B . Restricting the parameter space explored to fixed values of B (i.e. instead of marginalising over all B values) favours different parts of the

Parameter	Global peak	68%	95%
z_t	0.95	$0.75^{+0.25}_{-0.05}$	$0.75^{+0.50}_{-0.15}$
A	4.20	> 3.5	> 3.3
B	0.04	< 0.52	< 0.59

Table 3. Maximum likelihood parameters for the extragalactic background light fit. The parameters are defined in equation 10. The 68% and 95% confidence bounds quoted are in each case marginalised over the other two parameters with an $2 < A < 5$ top-hat prior assumed. The global maximum is not affected by the prior on A .

contoured region: low B values favour the low A / high z_t region of the contours, while high B values favour the high A / low z_t region.

These constraints on the A and z_t parameter space are determined only from the comparison of the extragalactic background light with our tightly-constrained determination of the local spectral luminosity density, and made no use of (e.g.) the empirical constraints available on Ω_* or the $850\mu\text{m}$ source counts. These latter two constraints are overplotted in figure 13, for comparison with our extragalactic background light constraint. The $850\mu\text{m}$ counts assume pure luminosity evolution to $z = z_t$, in concordance with galaxy evolution at other wavelengths, and pure density evolution thereafter. Ω_* is determined from the local $60\mu\text{m}$ luminosity density ρ_{60} with the following relation (Rowan-Robinson 2001):

$$\Omega_* = 10^{-11.13} \xi h^{-2} \frac{\rho_{60}}{1L_{\odot} \text{Mpc}^{-3}} \frac{t_0}{10\text{Gyr}} \quad (11)$$

Some source count models of the sub-mm population have had difficulty in reproducing this Ω_* constraint (e.g. Blain et al. 1999), though in our case we show below that there is good agreement with our extragalactic background light modelling.

Figure 13 can easily be translated into evolution tracks in the cosmic star formation history, as shown in figure 15. Note however that the parameters in figure 13 are correlated, so that the error on the comoving star formation rate at one redshift is correlated with that at another redshift, a fact which is rarely recognised (e.g. Gispert et al. 2000). Figure 13 is therefore the “least-misleading” presentation of our constraints on the cosmic star formation history.

An alternative to pure luminosity evolution sometimes used in the phenomenology of quasar evolution is to assume that the decline at the highest redshifts is pure density evolution, while still treating the increase from zero redshift as preserving pure luminosity evolution. We found this made only a modest difference to our $850\mu\text{m}$ 8mJy counts. These predictions are not plotted in figure 13 for clarity, but in the $B = 0.04$ and $B = 0.6$ cases, they are roughly equivalent to a 1σ shift in the observed 8mJy counts (i.e., a slight shift down and to the left of the 8mJy counts constraint). The $B = 0$ and $B = 1$ cases are non-evolving above the threshold redshift z_t , so there

are no changes in the 8mJy $850\mu\text{m}$ counts predictions in these cases. Also, the Ω_* predictions in general depend only on the evolution in luminosity density, and not on the comparative evolution of luminosities and number densities.

The global peak of the likelihood in this parameter space is given in table 3, as are the 68% and 95% confidence bounds on each of the parameters when marginalised over the other two. We found acceptable fits with unphysically large values of A and very small values of z_t (see figure 13) so we adopted an $2 < A < 5$ top-hat prior in calculating the confidence bounds. This did not affect the global peak. Figure 14 shows the global best fit to the extragalactic background light data. A notable requirement of these fits is a rapid decline in comoving star formation density above $z_t \simeq 1$. This is confirmed both by the Ω_* and $850\mu\text{m}$ counts constraints, both of which are overpredicted in a $B = 1$ model (i.e. $f(z) = \text{constant}$ above $z = z_t$).

However, this star formation history is immediately seen to be in conflict with determinations of the redshift distribution of sub-millimetre galaxies (e.g. Chapman et al. 2003) as well as other direct determinations. How can these be reconciled? We will address this in the following section.

4 DISCUSSION AND CONCLUSIONS

Our determinations of the local far-infrared to sub-mm luminosity functions span sufficient luminosity range to identify the convergence in the local spectral luminosity density. In particular, the $850\mu\text{m}$ local luminosity density is found to be $7.3 \pm 0.2 \times 10^{19} h_{65} \text{W Hz}^{-1} \text{Mpc}^{-3}$ solving the “sub-mm Olbers’ Paradox” (Dunne et al. 2000). Our SED predictions rely on the extrapolation of the SLUGS colour-colour relations, both to higher and lower $60\mu\text{m}$ luminosities. Although we have no reason to suspect this extrapolation is invalid, direct tests with sub-mm photometry of low and high $60\mu\text{m}$ galaxies are a key test of our methodology and are an attractive alternative to large photometric campaigns of local galaxies for constraining the local sub-mm luminosity functions.

Using only the observed extragalactic background light and our local spectral luminosity density, we derive a conditional constraint on the $z < 2$ obscured cosmic star formation history consistent with $(1+z)^A$ evolution with $A > 3.5$ to $z \simeq 1$. We find that the extragalactic background light, the $850\mu\text{m}$ 8mJy source counts, and the Ω_* constraints all independently point to a decline in the comoving star formation rate at $z > 1$. However, this is at variance with direct determinations, and with the constraints on the redshift distribution of sub-millimetre galaxies (e.g. Chapman et al. 2003).

Perhaps the most uncertain of our assumptions is equation 9. This equation is true in a very gen-

Figure 16. Predicted high-redshift extragalactic source counts at $170\mu\text{m}$ and $850\mu\text{m}$ for the $A = 3.75$, $B = 0.04$, $z_t = 1.0$ pure luminosity evolution model, compared to the observed counts from Barger et al. (1999), Dole et al. (2001), Scott et al. (2002), Cowie et al. (2002), and Webb et al. (2003). Note that *none* of these observed counts were used as constraints in generating the model, except the $850\mu\text{m}$ 8mJy count. In the $850\mu\text{m}$ plot, each of the data points are from a different source and (unusually for a cumulative source count plot) are therefore *statistically independent*, with the exception of the $> 8\text{mJy}$ data which is all from Scott et al. (2002). The overprediction of the faint $850\mu\text{m}$ counts is further indication that the evolution at faint luminosities is less strong than that at bright luminosities (section 4).

eral class of cases, including pure luminosity evolution, pure density evolution and any mixed luminosity/density evolution models (i.e. those in which the shape of the luminosity function is invariant with redshift, but not the break luminosity or the number density at the break). However, if (for example) the high-luminosity sub-millimetre galaxies evolve more quickly than their low-luminosity counterparts, then equation 9 will not hold. Stronger evolution at the high-luminosity end would give the comoving luminosity density a warmer colour temperature at high redshift, which in turn would permit higher numbers of sub-millimetre galaxies at high redshift without vi-

olating the extragalactic background light constraint. The warmer colour temperature may also explain why our models fall short of the data at $140\mu\text{m}$ (figure 14), though this may also be due to our redshifted SEDs being less well-constrained at the shortest wavelengths. The Ω_* constraint would also be alleviated, since the extrapolation to galaxies with lower luminosities would yield less additional star formation.

A further indication that the evolution may be stronger at high luminosities is provided by the predicted blank-field high-redshift source counts at $170\mu\text{m}$ and $850\mu\text{m}$, shown in figure 16. It is important to stress that *none* of the observed source

counts in this figure were used as a constraint on the model, except the $850\mu\text{m}$ 8mJy count. While the observed $170\mu\text{m}$ and bright $850\mu\text{m}$ counts are both encouragingly well-reproduced by the model, the faint $850\mu\text{m}$ source counts are over-predicted. Suppressing the strength of evolution in the less luminous population would have the effect of reducing the predicted $850\mu\text{m}$ counts at the faint end.

An alternative solution to alleviating the constraints on Ω_* is that the initial mass function is more top-heavy at high redshifts. The infrared luminosities are dominated by $\gtrsim 6M_\odot$ stars (Condon 1992), so altering the initial mass function can have a strong effect on the Ω_* calculation while leaving the extragalactic background and source count predictions roughly intact. There are good *prima facie* reasons for supposing this might be the case (e.g. Larson 1998 and references therein), though if it were to entirely explain the discrepancy with the $850\mu\text{m}$ redshift distribution, the top heavy initial mass function would have to exist in low luminosity high-redshift galaxies, as well as ultraluminous high-redshift galaxies.

Within the cosmic star formation histories $f(z)$ we have considered, we can therefore conclude that the initial mass function is very different at high redshift, and/or some differential evolution is *required*; all pure luminosity, pure density and mixed luminosity/density evolution models are excluded by the $850\mu\text{m}$ blank-field survey redshift distributions if the initial mass function is the same at high redshift. Furthermore, comparison with the faint $850\mu\text{m}$ source counts already indicates the presence of differential evolution.

The issue of mm-wave/sub-mm/radio photometric redshifts is very timely given the advent of the SHADES survey (van Kampen et al. in prep., Mortier, Serjeant et al. in prep.), which will combine SCUBA and BLAST data with the aim of obtaining photometric redshifts accurate to $\Delta z \simeq 0.5$. The accuracies which are obtainable are still the subject of debate in the literature (e.g. Hughes et al. 2002, Blain et al. 2003) and are limited by the availability of local templates. It would be interesting to address the photometric redshift accuracy from the point of view of our SED ensemble. However, our results have already indicated that local ultraluminous galaxies may not necessarily be templates for the high-z ultraluminous systems being found by sub-mm blank-field surveys. The photometric redshifts will therefore need careful calibration against spectroscopic redshifts (e.g. Chapman et al. 2003), obtained for example using Spitzer identifications (e.g. Egami et al. 2004, Serjeant et al. 2004, Ivison et al. 2004, Frayer et al. 2004, Charmandaris et al. 2004).

ACKNOWLEDGEMENTS

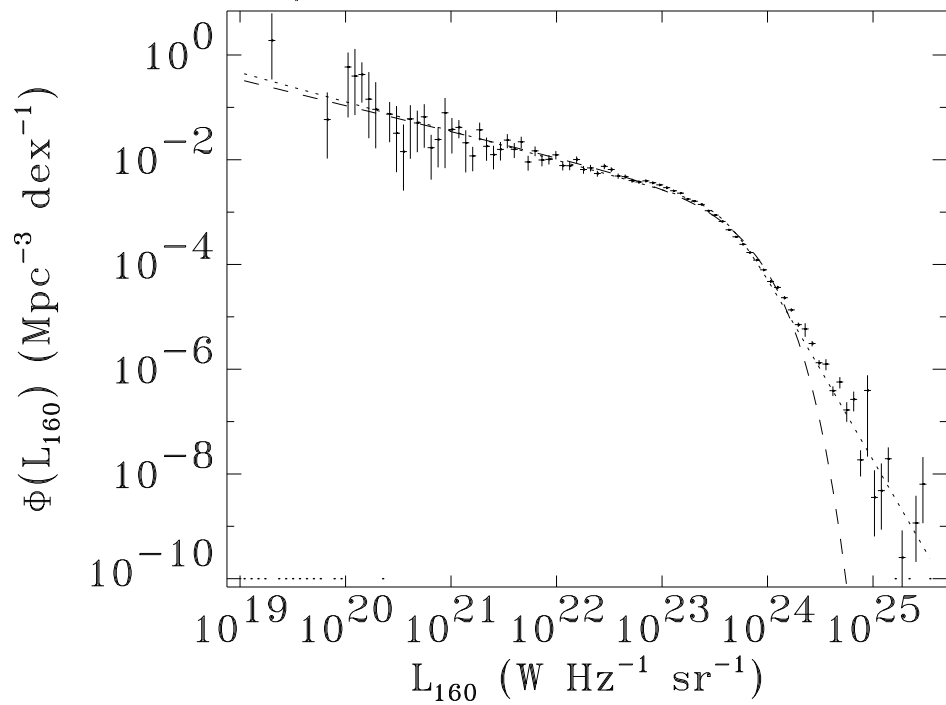
We would like to thank the referee, Eli Dwek, for many helpful suggestions and clarifications to this paper. This work was supported in part by PPARC (grant numbers GR/K98728, PPA/G/S/2001/00120, and PPA/V/S/2000/00563) and the Nuffield Foundation (grant number NAL/00529/G). The authors acknowledge the data analysis facilities provided by the Starlink Project which is run by CCLRC on behalf of PPARC.

REFERENCES

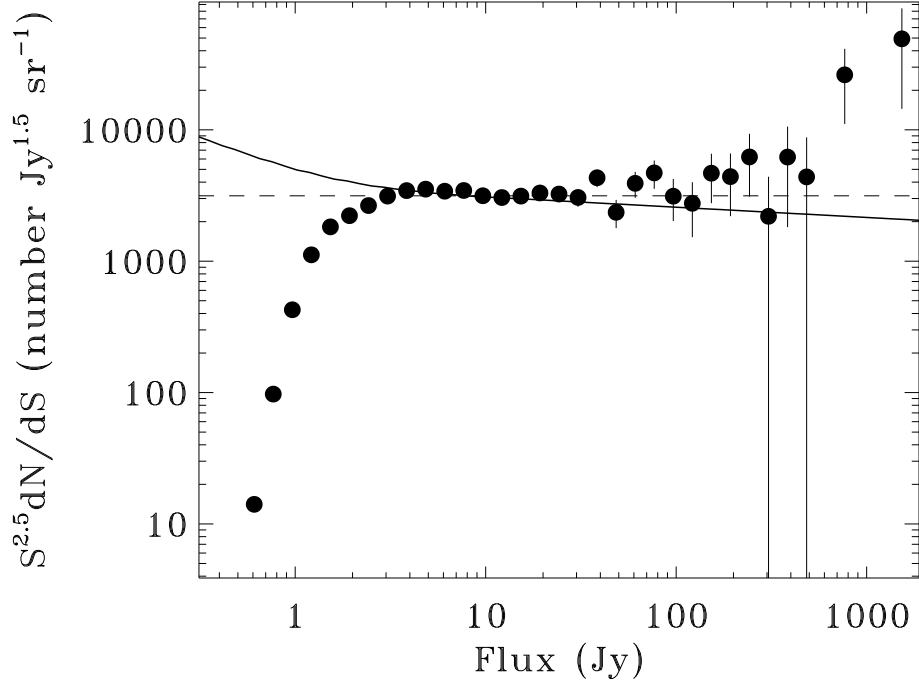
- Andreani, P., & Franceschini, A., 1996 MNRAS 283, 85
 Aretxaga, I., Hughes, D., Gaztanaga, E., Chapin, E., Dunlop, J., 2002, preprint astro-ph/0205313
 Barger, A.J., Cowie, L.L., Sanders, D.B., 1999, ApJ 518, L5
 Blain, A.W., Jameson, A., Smail, I., Longair, M.S., Kneib, J.-P., Ivison, R.J., 1999 MNRAS 309, 715
 Blain, A.W., Barnard, V.E., Chapman, S.C., 2003 MNRAS 338, 733
 Chapman, S.C., Helou, G., Lewis, G.F., Dale, D.A., 2003, preprint astro-ph/0301233
 Charmandaris, V., et al., 2004, ApJS Spitzer Special Issue, in press
 Condon, J.J., 1992, ARA&A, 30, 575
 Cowie, L.L., Barger, A.J., & Kneib, J.-P., 2002, AJ, 123, 2197
 Dale, D.A., Helou, G., Contursi, A., Silbermann, N.A., Kolharar, S., 2001, ApJ 549, 215
 Dale, D.A., Helou, G., 2002, ApJ 576, 159
 Dole, H., et al., 2001, A&A 372, 364
 Domingue, D.L., Keel, W.C., Ryder, S.D.; White, R.E. III, 1999, AJ 118, 1542
 Dunlop, J., 2001, in Deep millimeter surveys : implications for galaxy formation and evolution, Proceedings of the UMass/INAOE conference, University of Massachusetts, Amherst, MA, USA, 19-21 June 2000. Published by Singapore: World Scientific Publishing, 2001. xi, 207 p. Edited by James D. Lowenthal, and David H. Hughes. ISBN: 9810244657, p.11
 Dunne, L., Eales, S., Edmunds, M., Ivison, R., Alexander, P., Clements, D.L., 2000 MNRAS 315, 115
 Dunne, L., & Eales, S.A., 2001 MNRAS 327, 697
 Dwek, E., et al., 1998, ApJ 508, 106
 Eales, S., Lilly, S., Webb, T., Dunne, L., Gear, W., Clements, D., Yun, M., 2000 AJ 120, 2244
 Efstathiou, A., & Rowan-Robinson, M., 2002, MNRAS submitted
 Efstathiou, A., Rowan-Robinson, M., Siebenmorgen, R., 2000 MNRAS 313, 734
 Egami, E., et al., 2004, ApJS Spitzer Special Issue, in press
 Frayer, D.T., et al., 2004, ApJS Spitzer Special Issue, in press
 Fixsen, D.J., Dwek, E., Mather, J.C., Bennett, C.L., Shafer, R.A., 1998 ApJ 508, 123
 Fox, M.J., et al. 2002 MNRAS 331, 839
 Glazebrook, K., et al., 2003, ApJ, 587, 55
 Gispert, R., Lagache, G., Puget, J.-L., 2000, A&A 360, 1
 Glenn, J., et al., 1998, SPIE 3357, 326
 Griffin, M.J., Swinyard, B.M., Vigroux, L., 2001, in The

- Promise of the Herschel Space Observatory. Eds. G.L. Pilbratt, J. Cernicharo, A.M. Heras, T. Prusti, & R. Harris. ESA-SP 460, p. 37
- Haas, M., Klaas, U., Coulson, I., Thommes, E., Xu, C., 2000, *A&A* 356, L83;
- Hauser, D.M., et al., 1998, *ApJ*, 508, 25
- Hauser, D.M., & Dwek, E., 2001, *ARA&A* 39, 249
- Holland, W., et al., 2002, *BAAS* 201, 121.02
- Hughes, D.H., et al., 2002 *MNRAS* 335, 871
- Hughes, D., Serjeant, S., Dunlop, J., Rowan-Robinson, M., et al., 1998
- Iverson, R.J., Smail, I., Barger, A.J., Kneib, J.-P., Blain, A.W., Owen, F.N., Kerr, T.H., Cowie, L.L., 2000, *MNRAS* 315, 209
- Iverson, R.J., et al., 2004, *ApJS Spitzer Special Issue*, in press
- Kaercher, H.J., & Baars, J.W., 2000, *SPIE* 4015, 155
- Kaviani, A., Haehnelt, M.G., Kauffmann, G., 2002, preprint (astro-ph/0207238)
- King, A.J., & Rowan-Robinson, M., 2003, *MNRAS* 339, 260
- Lagache, G., Abergel, A., Boulanger, F., Désert, F.X., Puget, J.-L., 1999, *A&A* 344, 322
- Lagache, G., Haffner, L.M., Reynolds, R.J., Tufte, S.L., 2000, *A&A* 354, 247
- Lagache, G., Dole, H., Puget, J.-L., 2003, *MNRAS* 338, 555
- Lamarre, J.M., et al., 2000, *ApL&C* 37, 161
- Lanzetta, K. M., Yahil, A., & Fernandez-Soto, A. 1996, *Nature*, 381, 759
- Larson, R.B., 1998, *MNRAS* 301, 569
- Lutz, D., et al. 2002 *A&A* 378, 70
- Madau P., Ferguson H.C., Dickinson M.E., Giavalisco M., Steidel C.C., Fruchter A., 1996, *MNRAS*, 283, 1388
- Oliver, S., et al., 2000, *MNRAS* 316, 749
- Peacock, J.A., 2000, *Cosmological Physics*, CUP, Cambridge.
- Pearson, C.P., Matsuhara, H., Onaka, T., Watarai, H., Matsumoto, T., 2001, *MNRAS* 324, 999
- Puget et al. 1996, *ApJ* 308, L5
- Rowan-Robinson, M., 2001, *ApJ* 549, 745
- Saunders, W., et al., 2000 *MNRAS* 317, 55
- Schlegel, D.J., Finkbeiner, D.P., Davis, M., 1998, *ApJ* 500, 525
- Schmidt, M., 1968, *ApJ* 151, 393
- Scott, S.E., et al. 2002 *MNRAS* 331, 817
- Serjeant, S., et al., 2001, *MNRAS*, 322, 262
- Serjeant, S., et al., 2003, *MNRAS*, 344, 887
- Serjeant, S., et al., 2004, *ApJS Spitzer Special Issue*, in press
- Siebenmorgen, R., Krügel, E., Chini, R., 1999, *A&A* 351, 495;
- Smail, I., Ivison, R., Blain, A., Kneib, J.-P., 2002, *MNRAS* 331, 495
- Shibai, H., 2002, *Advances in Space Research*, 30, 2089
- Soifer, B.T., Neugebauer, G., *AJ*, 101, 354
- Stickel, M., Lemke, D., Klaas, U., Beichman, C.A., Rowan-Robinson, M., Efstathiou, A., Bogun, S., Kessler, M.F., Richter, G., 2000, *A&A* 359, 865
- Takeuchi, T.T., Yoshikawa, K., Ishii, T.T., 2003, *ApJ*, 587, L89
- Thompson, R.I., Weymann, R.J., Storrie-Lombardi, L.J., 2001 *ApJ* 546, 649
- Trewhella, M., Davies, J.I., Alton, P.B., Bianchi, S., Madore, B.F., 2000 *ApJ* 543, 153
- Tucker, G.S., et al., 2004, *Advances in Space Research*, 33, 1793
- Webb, T.M., et al., 2003, *ApJ*, 587, 41

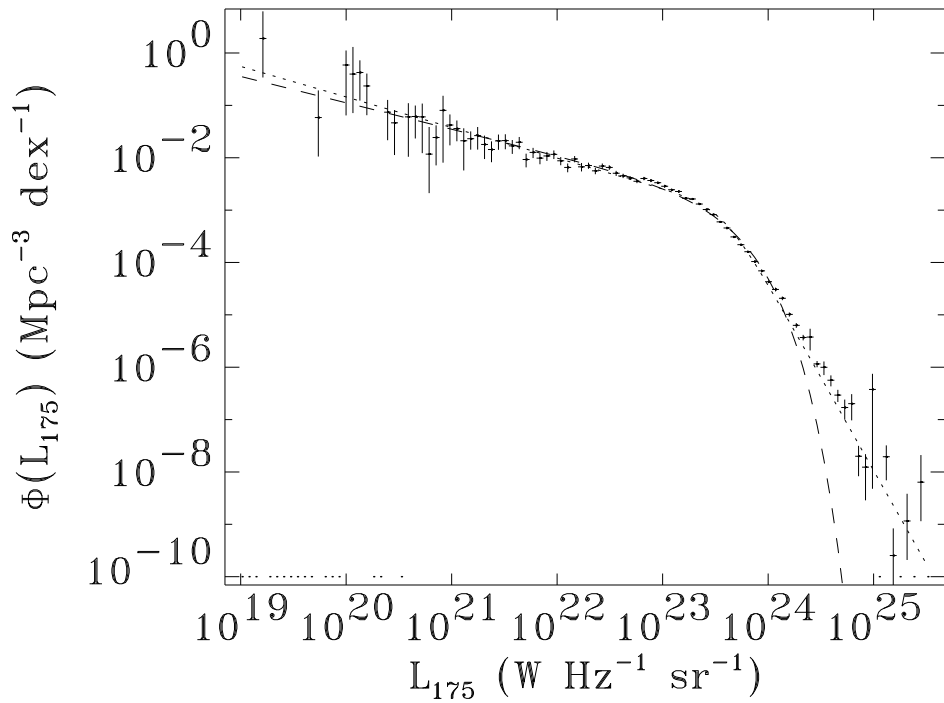
160 μ m Luminosity Function



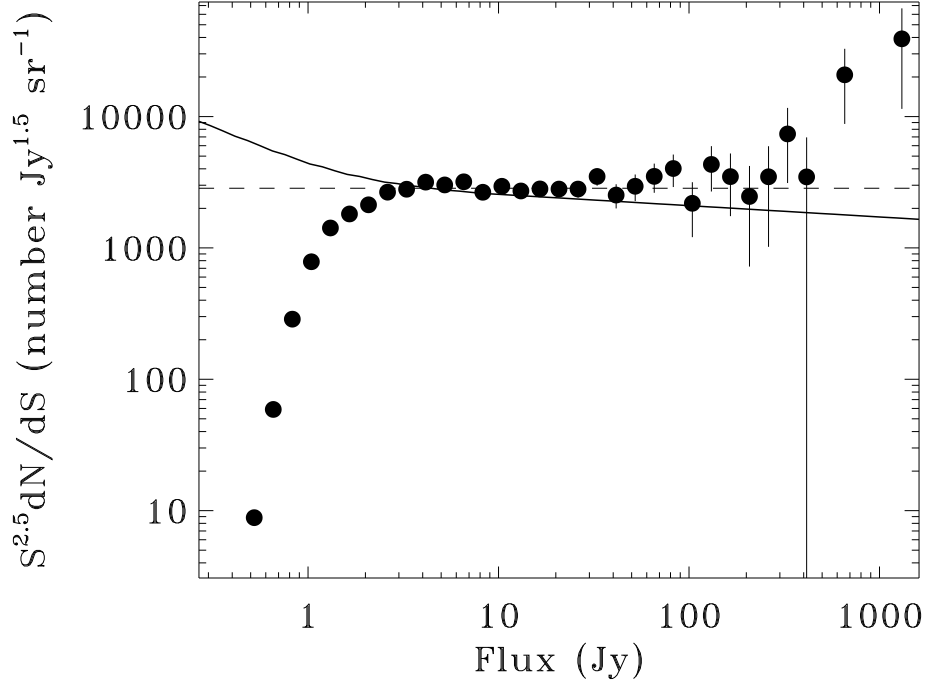
160 μ m Differential Source Counts



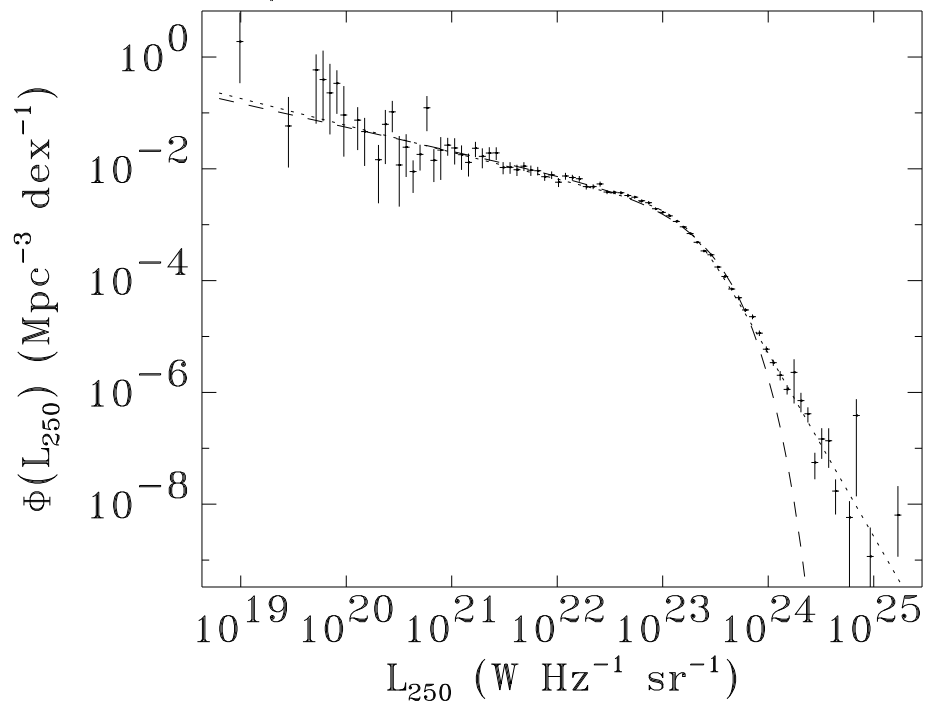
175 μ m Luminosity Function



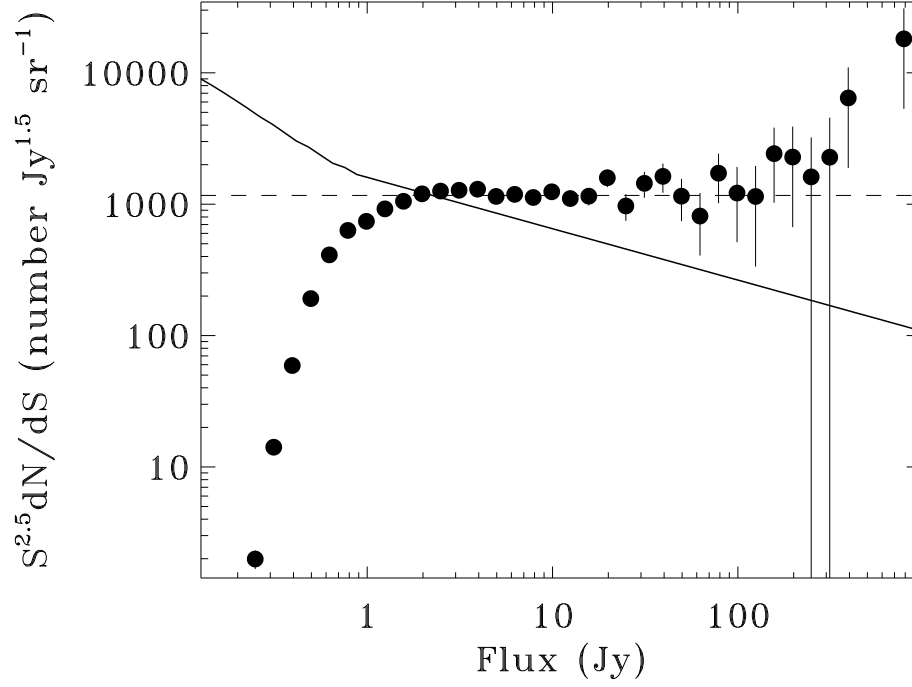
175 μ m Differential Source Counts



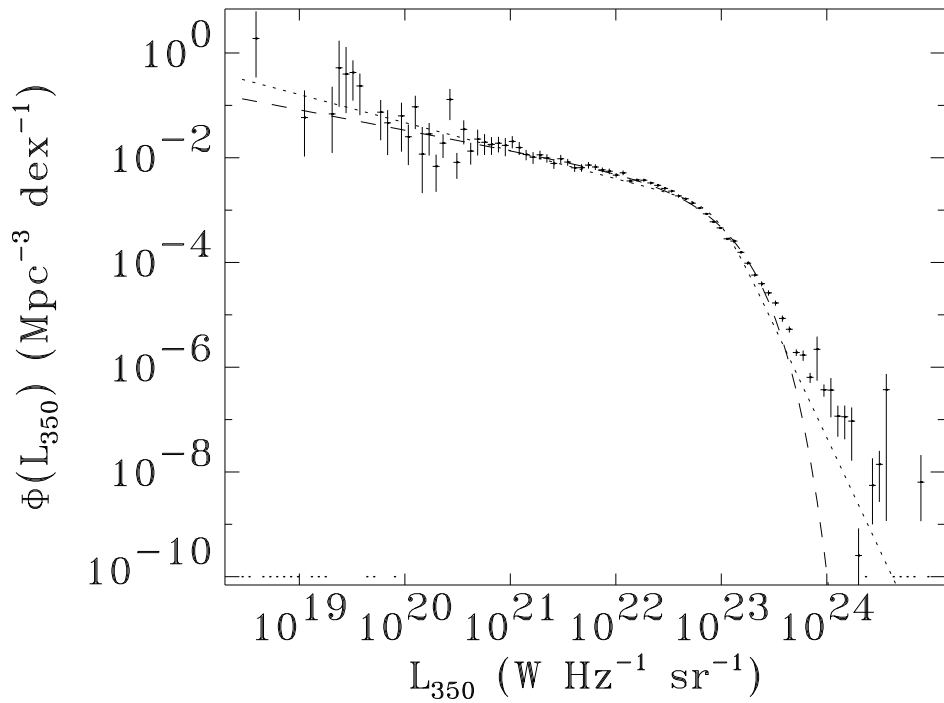
250 μ m Luminosity Function



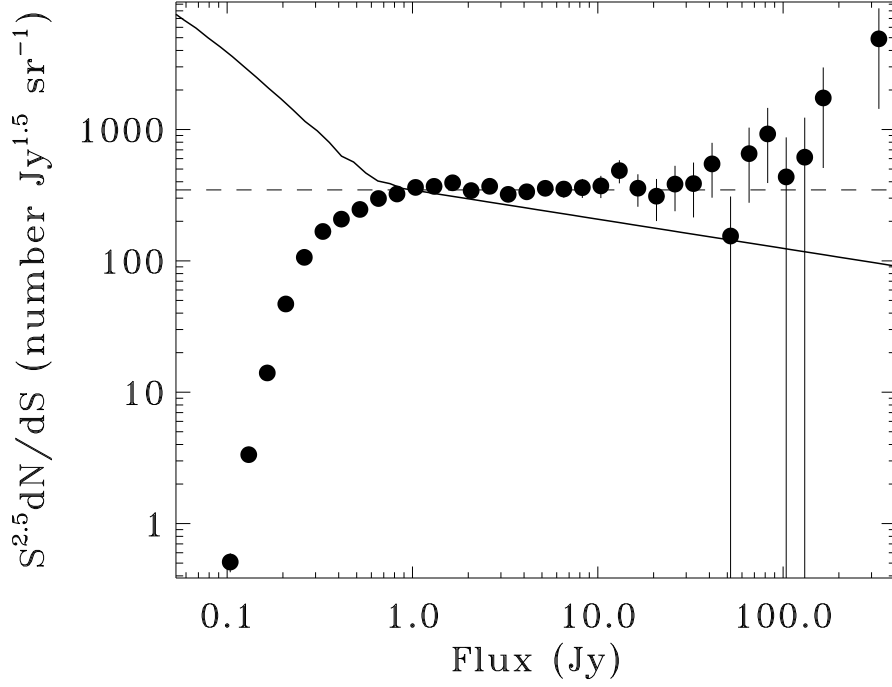
250 μ m Differential Source Counts



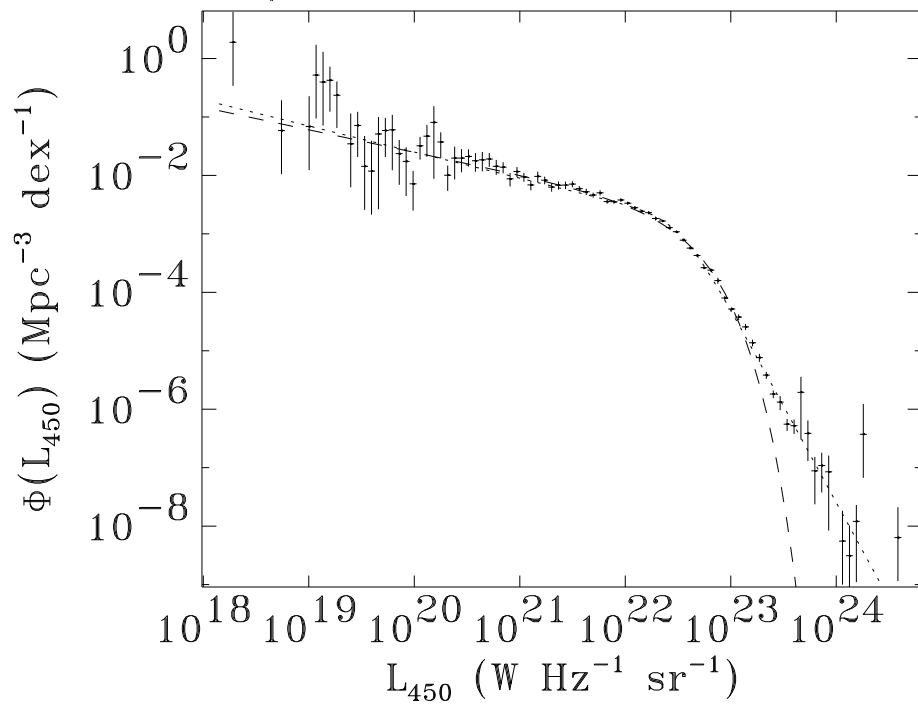
350 μ m Luminosity Function



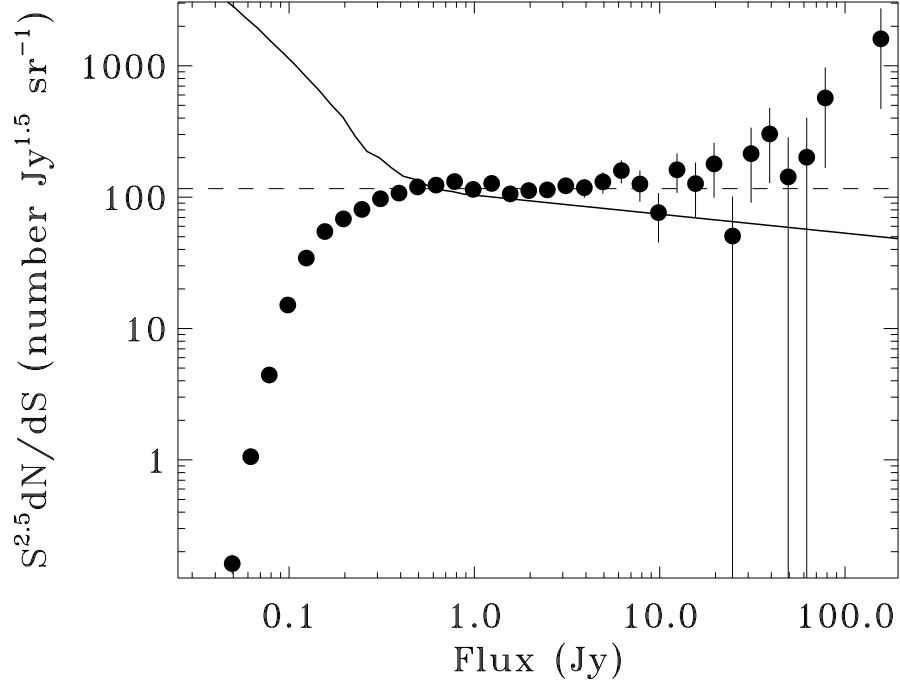
350 μ m Differential Source Counts



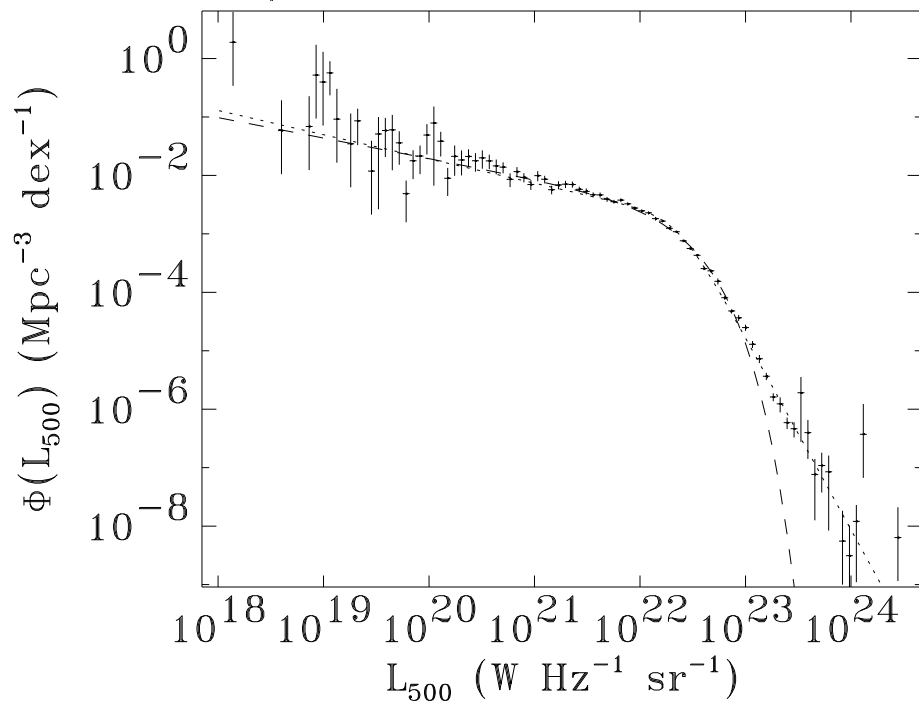
450 μ m Luminosity Function



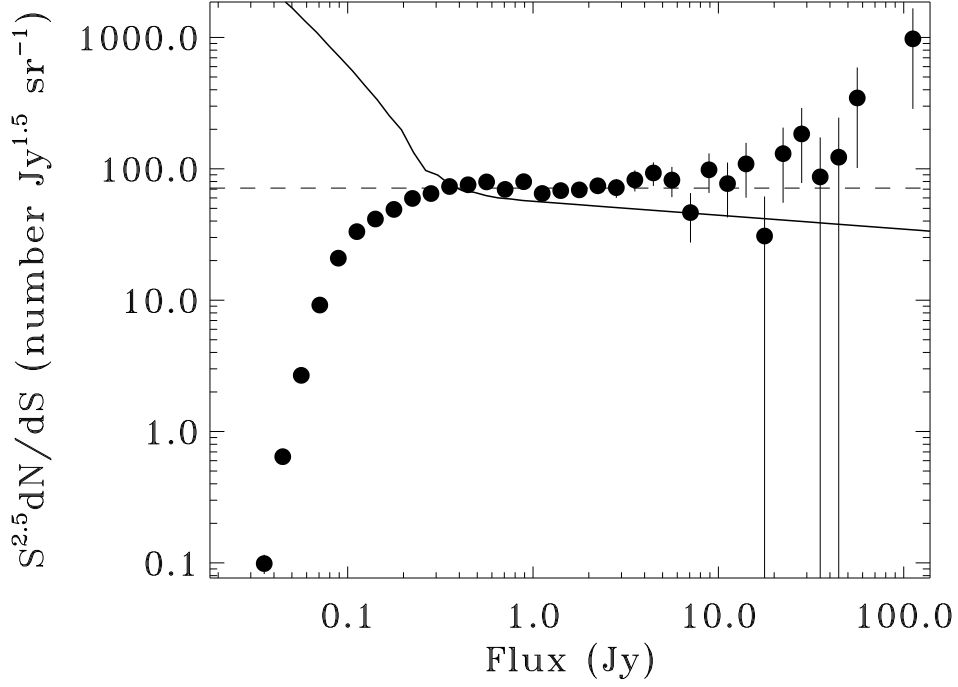
450 μ m Differential Source Counts



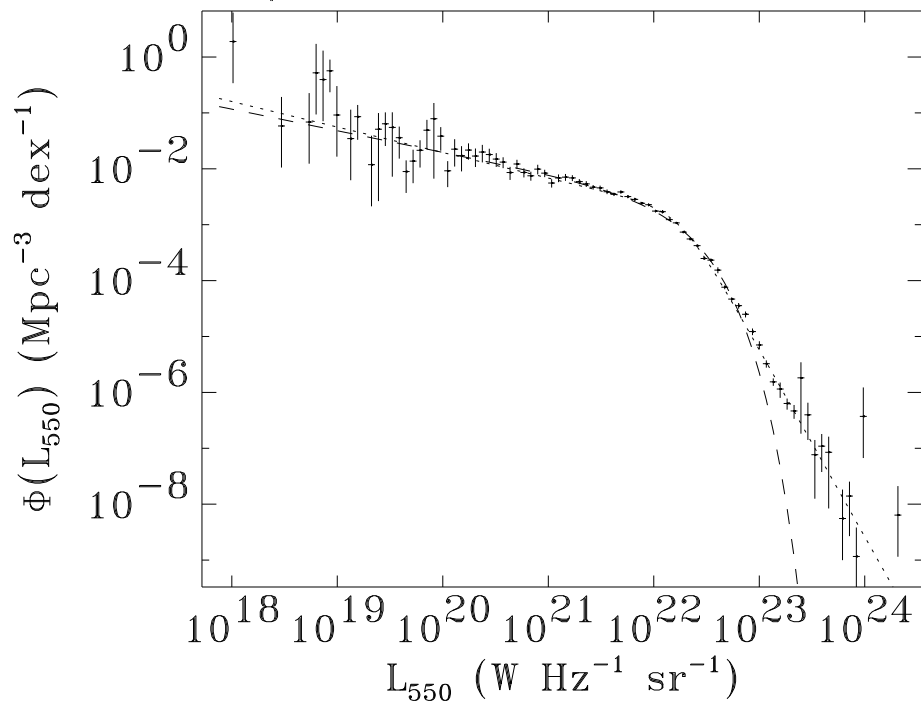
500 μ m Luminosity Function



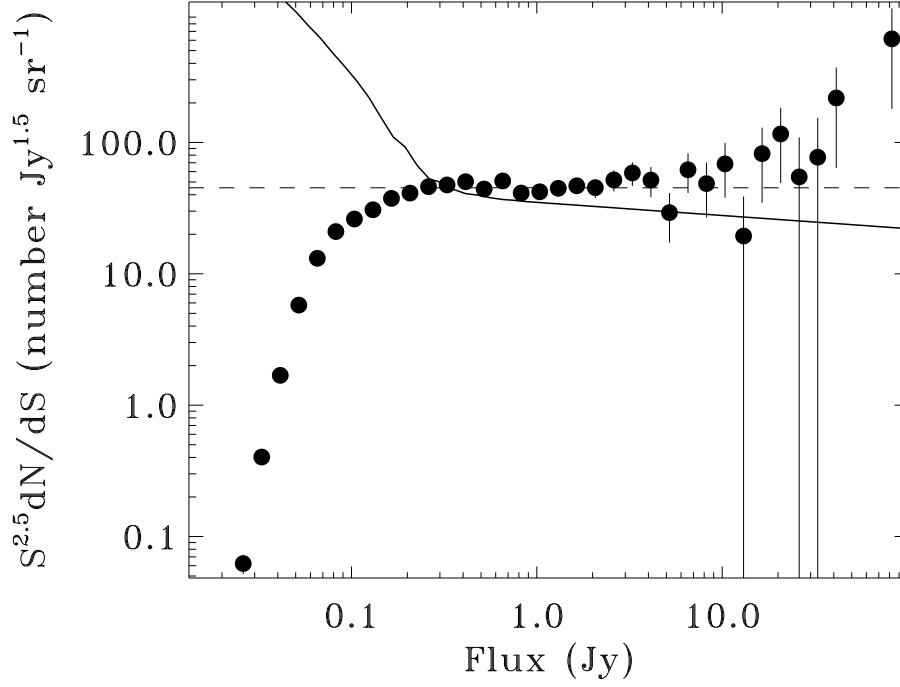
500 μ m Differential Source Counts



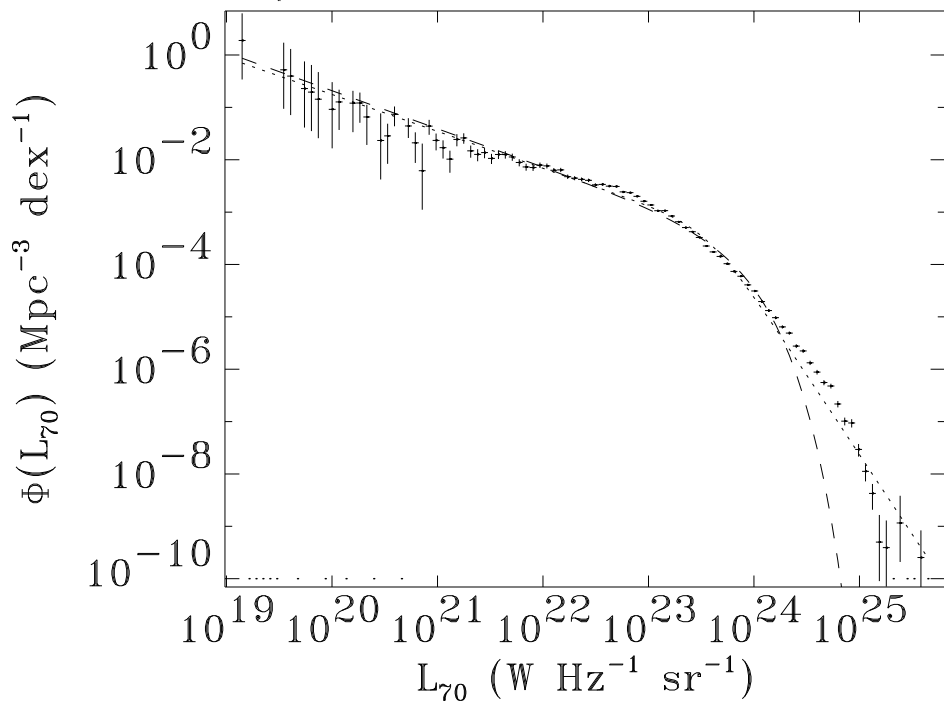
550 μ m Luminosity Function



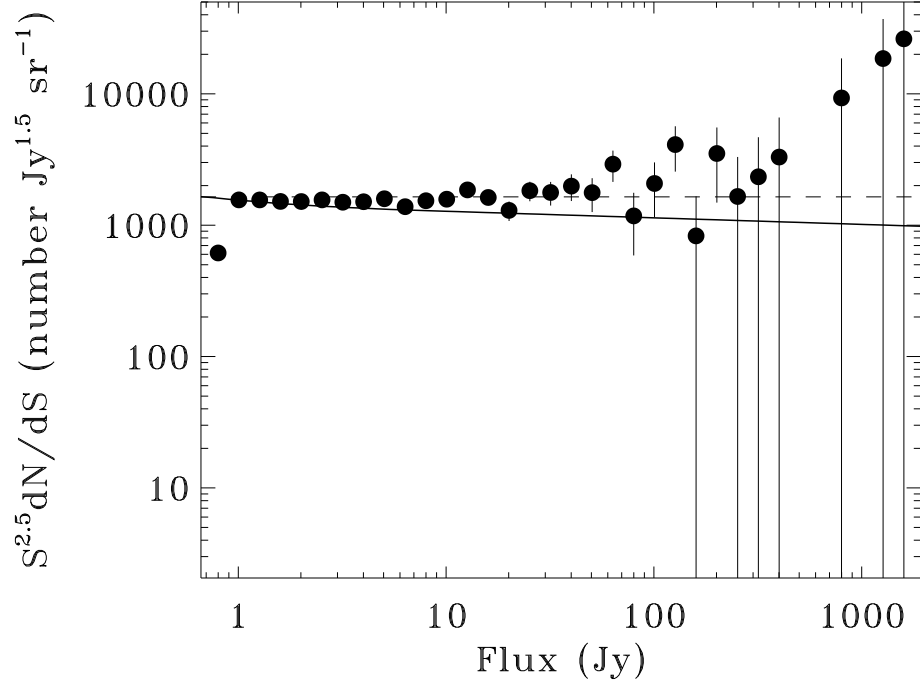
550 μ m Differential Source Counts



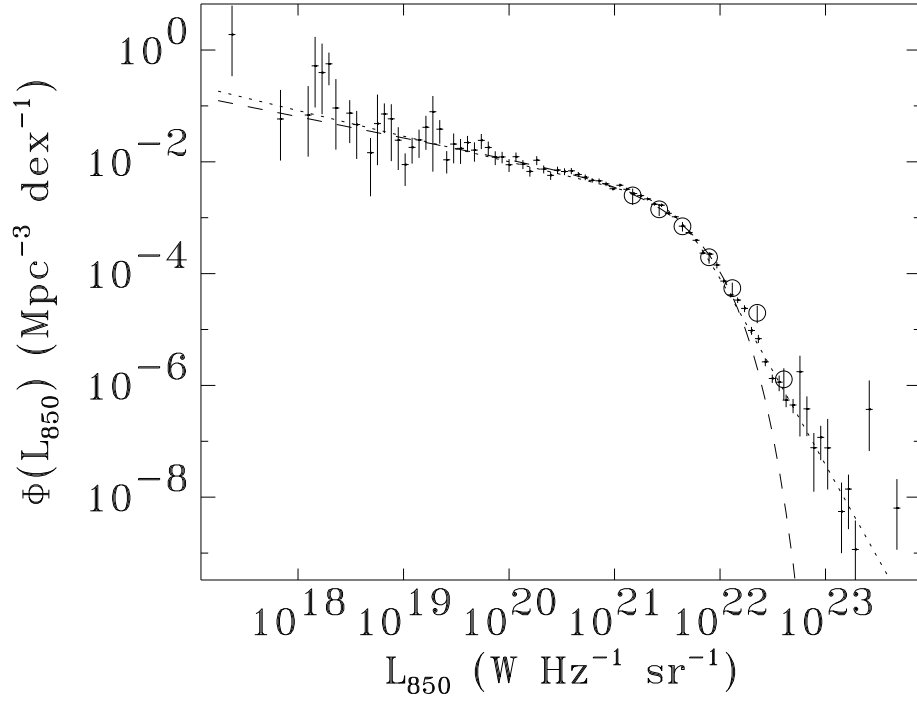
70 μ m Luminosity Function

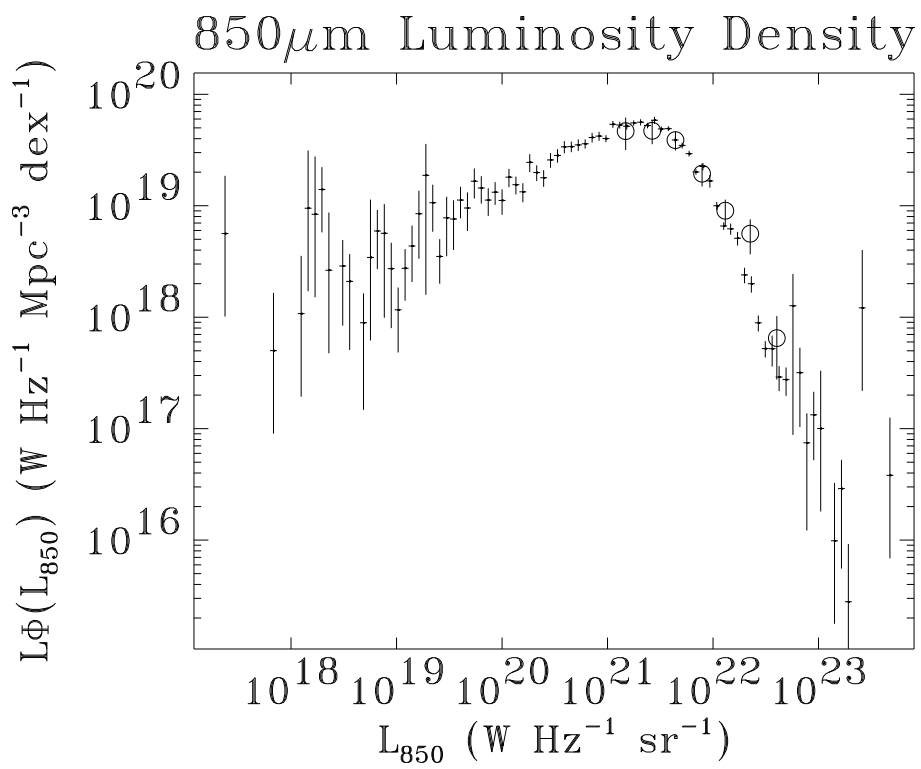


70 μ m Differential Source Counts

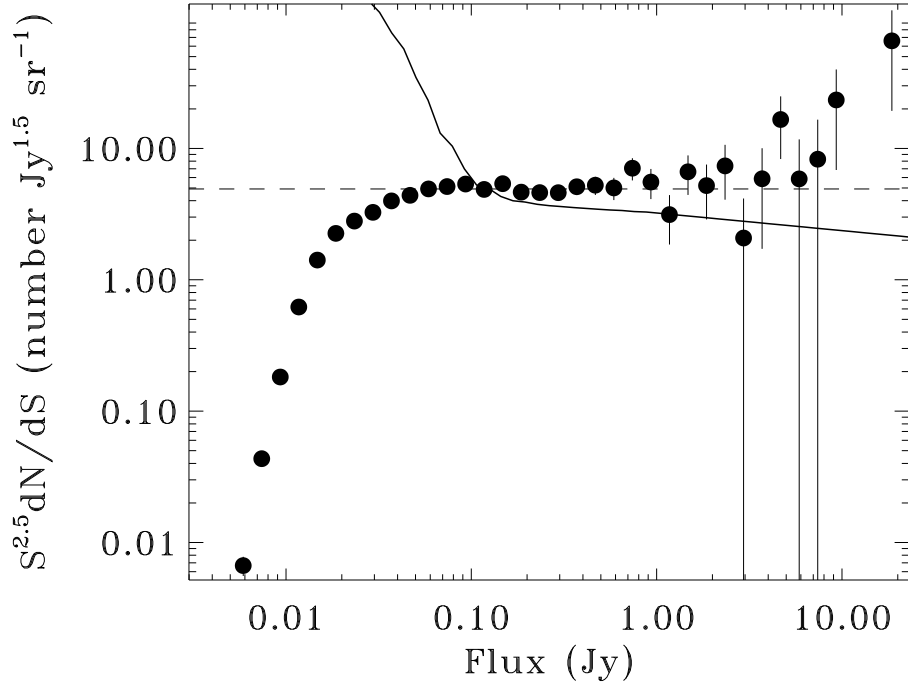


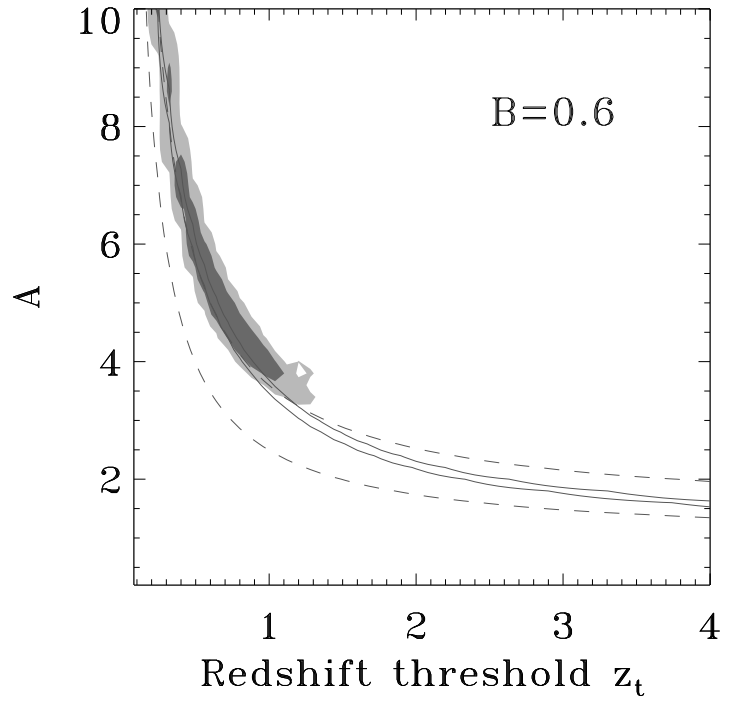
850 μm Luminosity Function

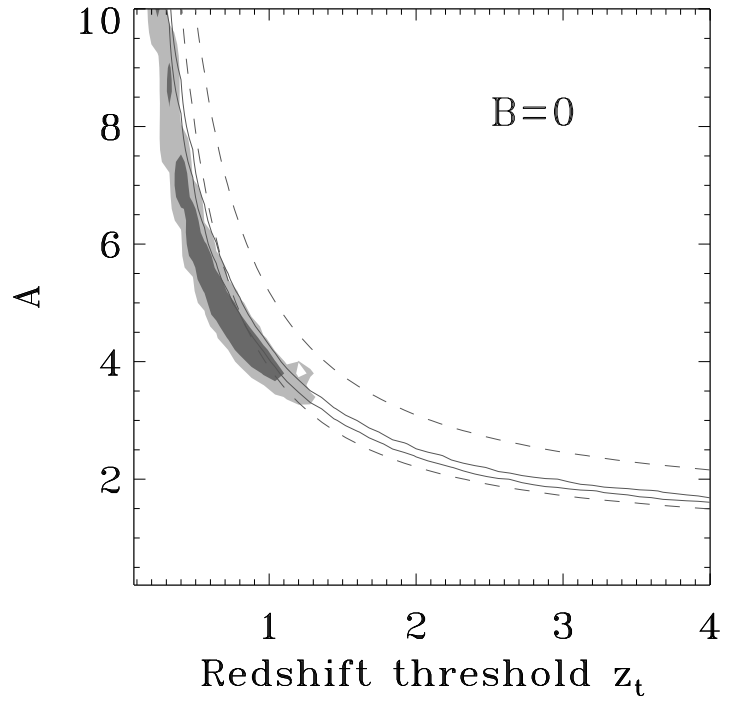


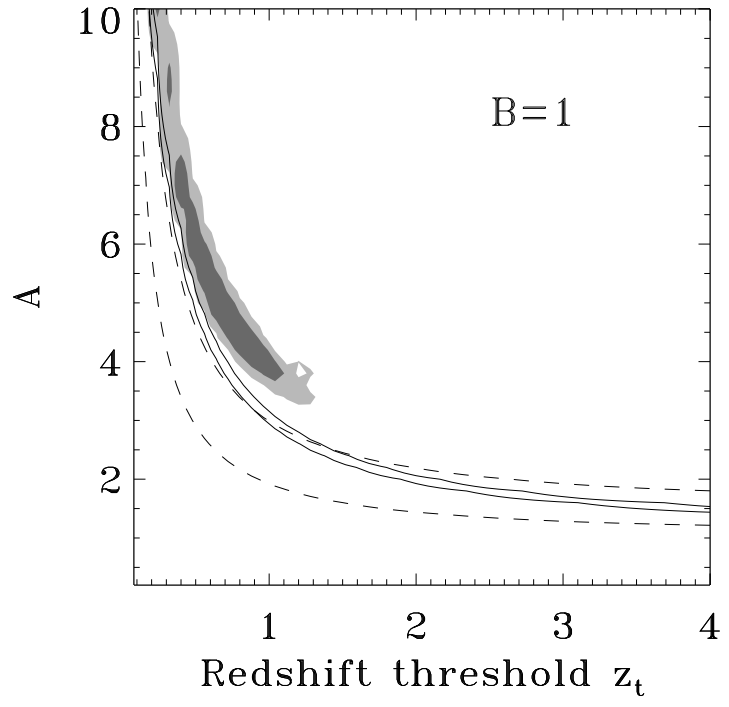


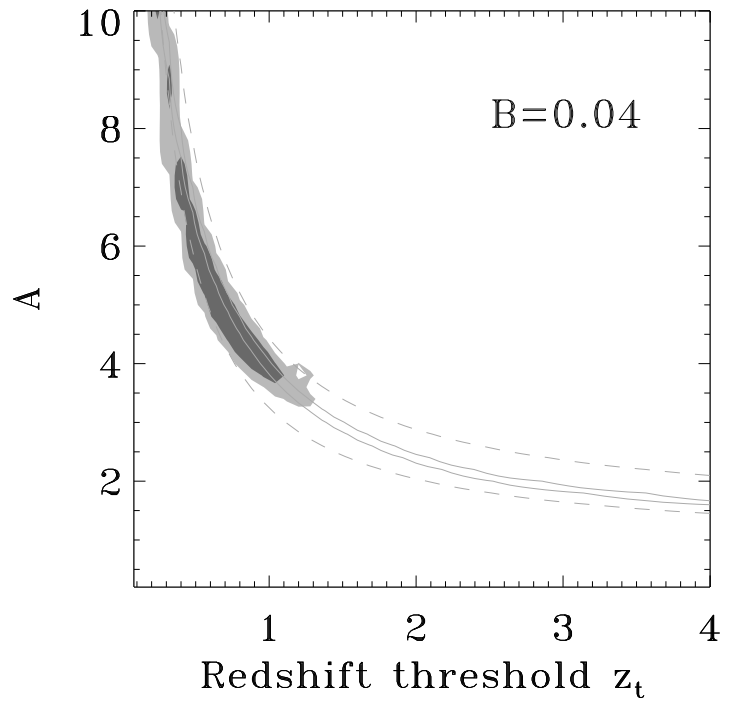
850 μ m Differential Source Counts



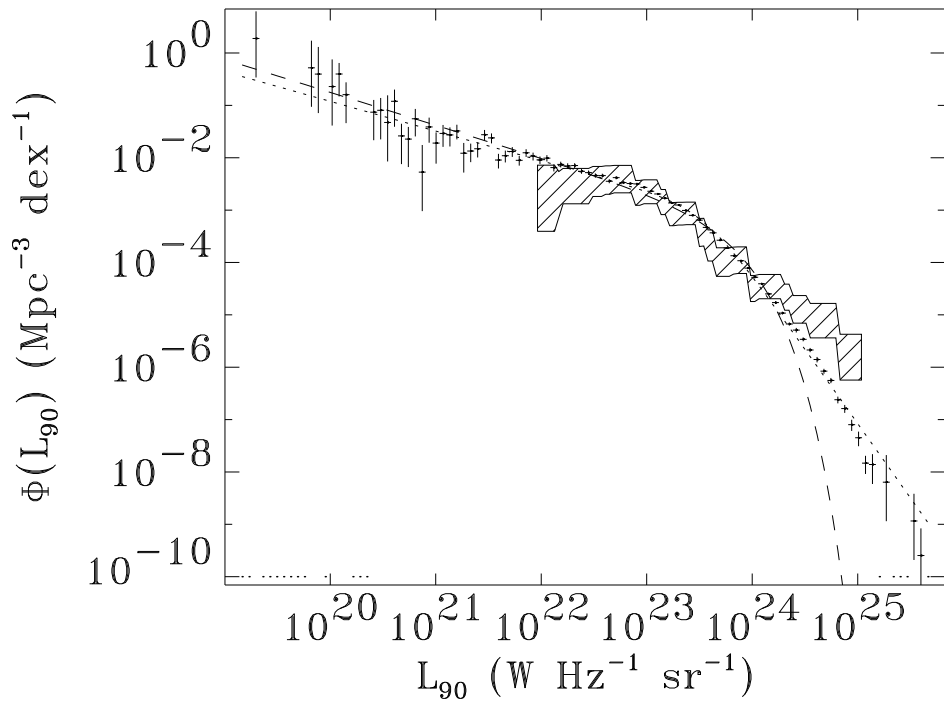




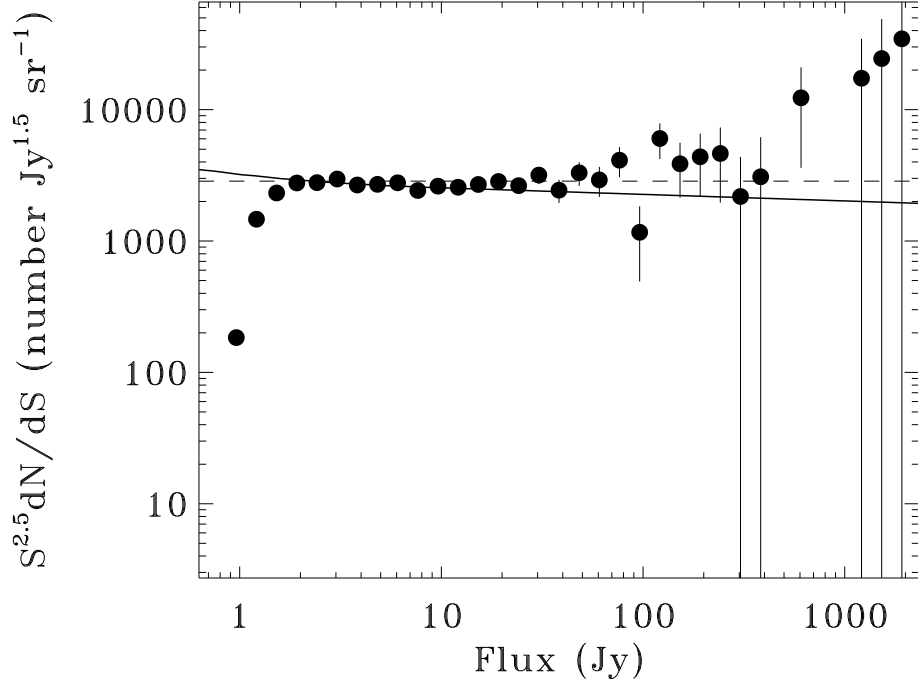


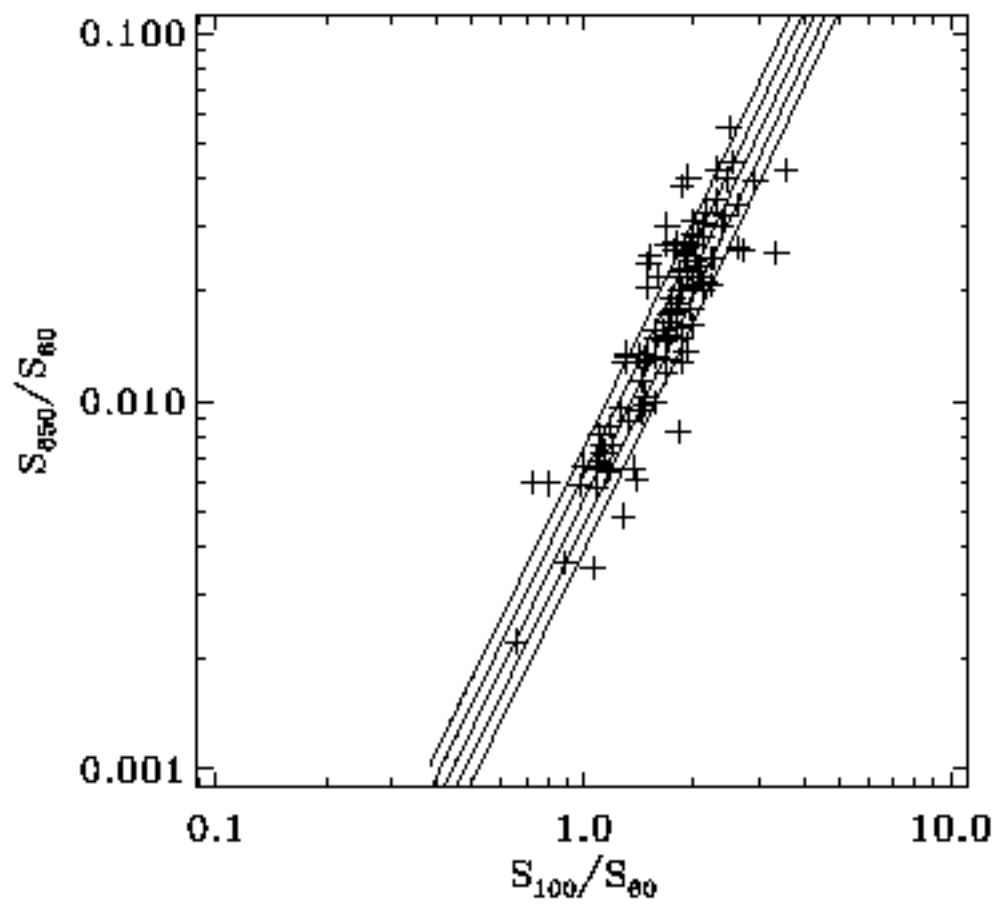


90 μ m Luminosity Function

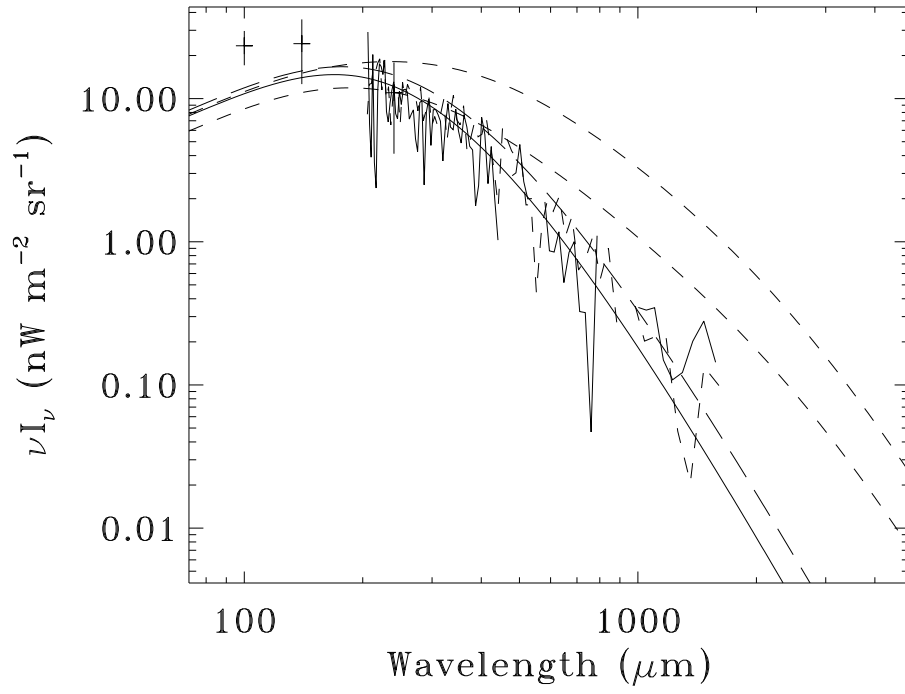


90 μ m Differential Source Counts

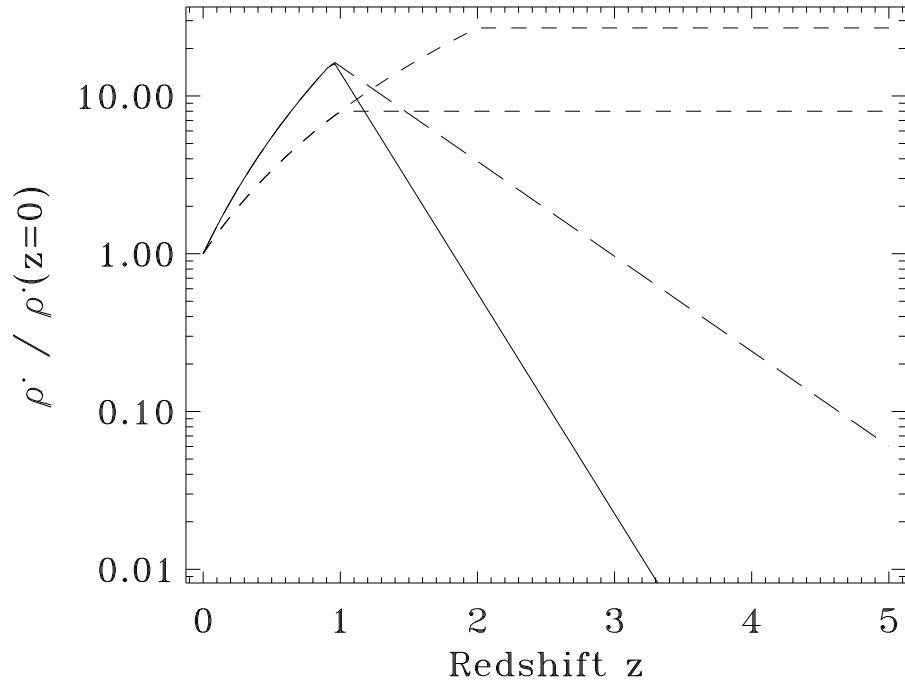




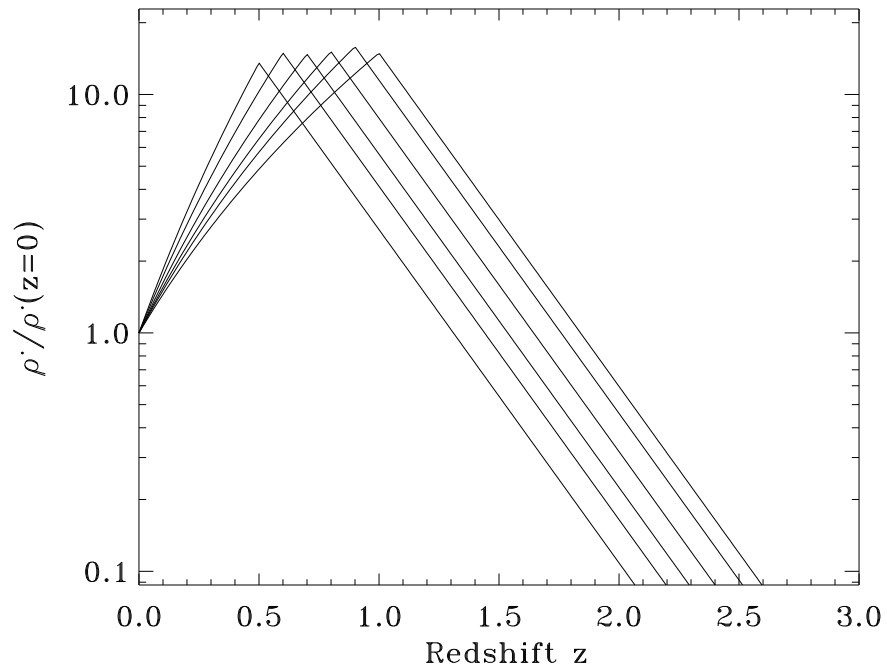
Extragalactic background light

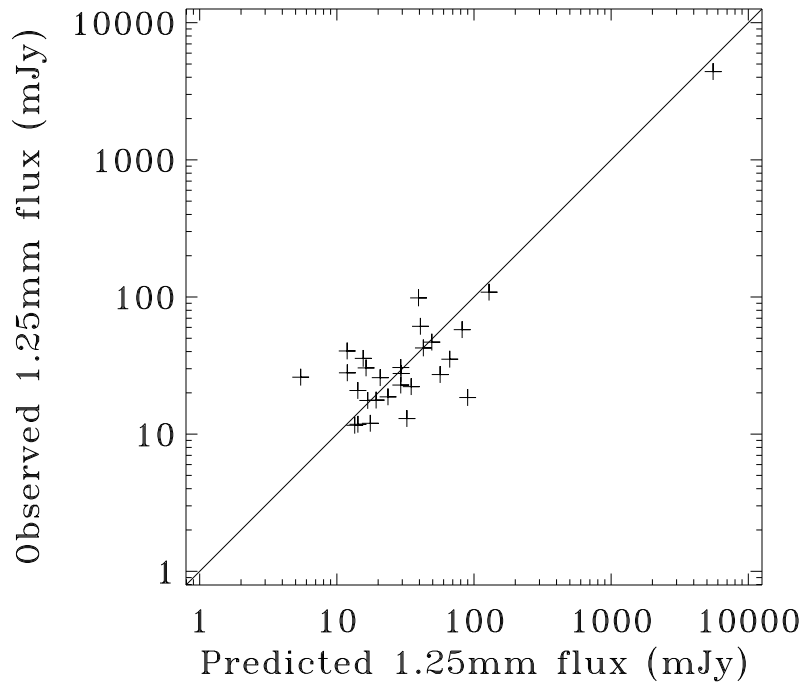


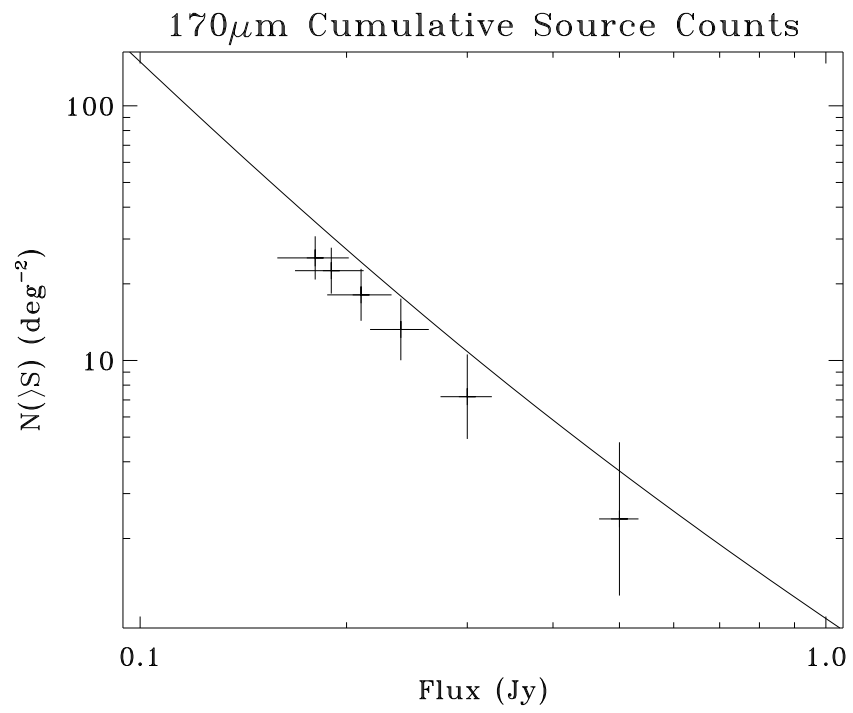
Cosmic star formation history

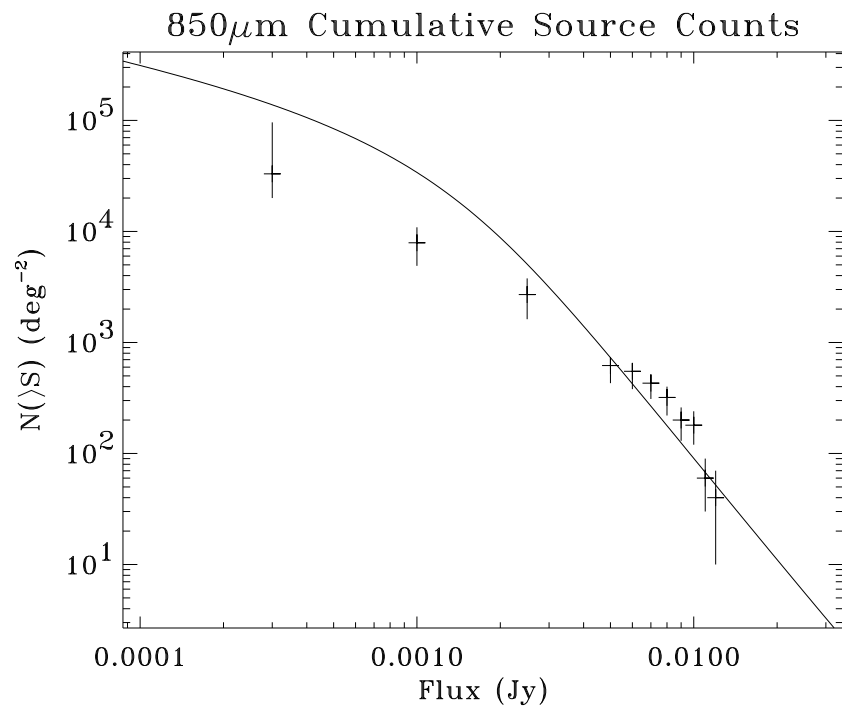


Cosmic star formation history, B=0.04

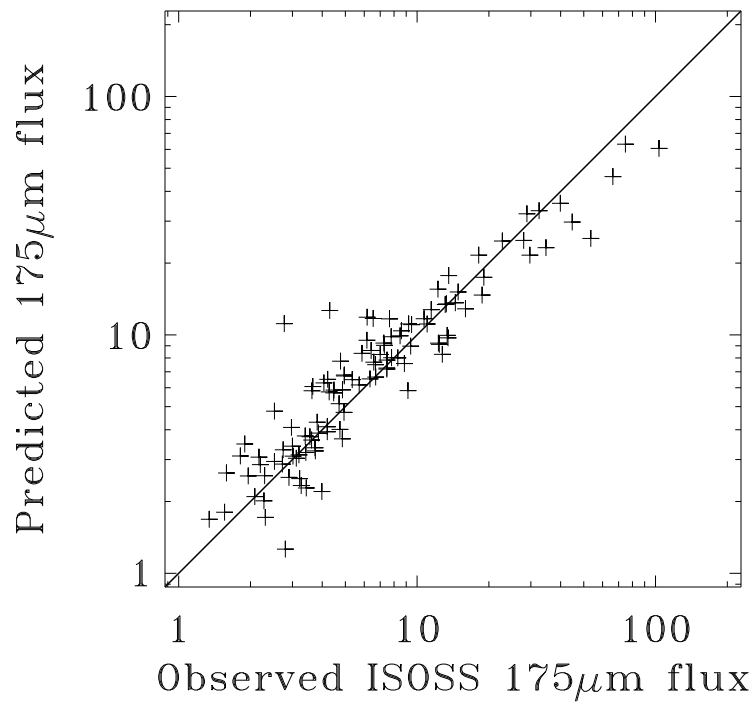




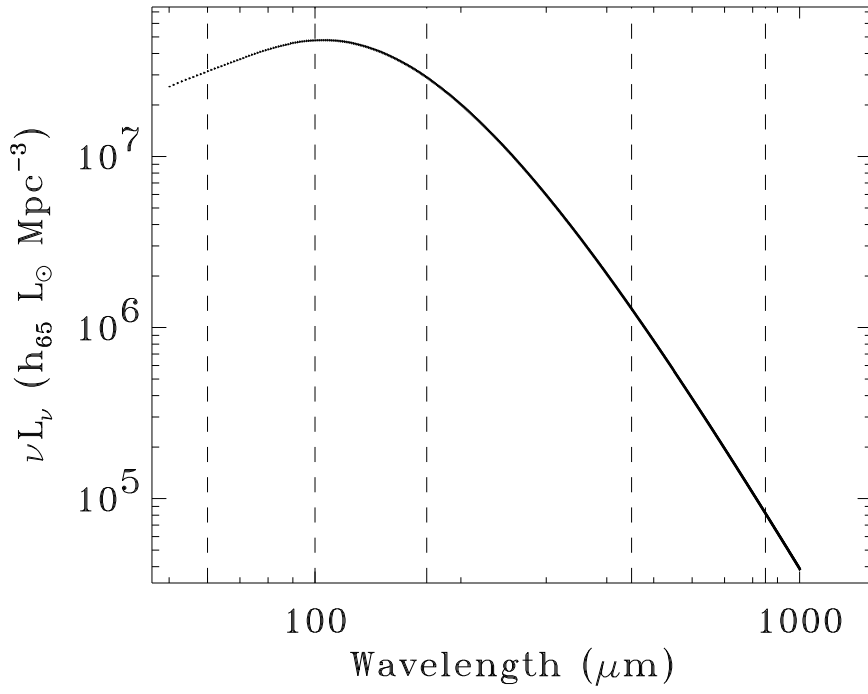




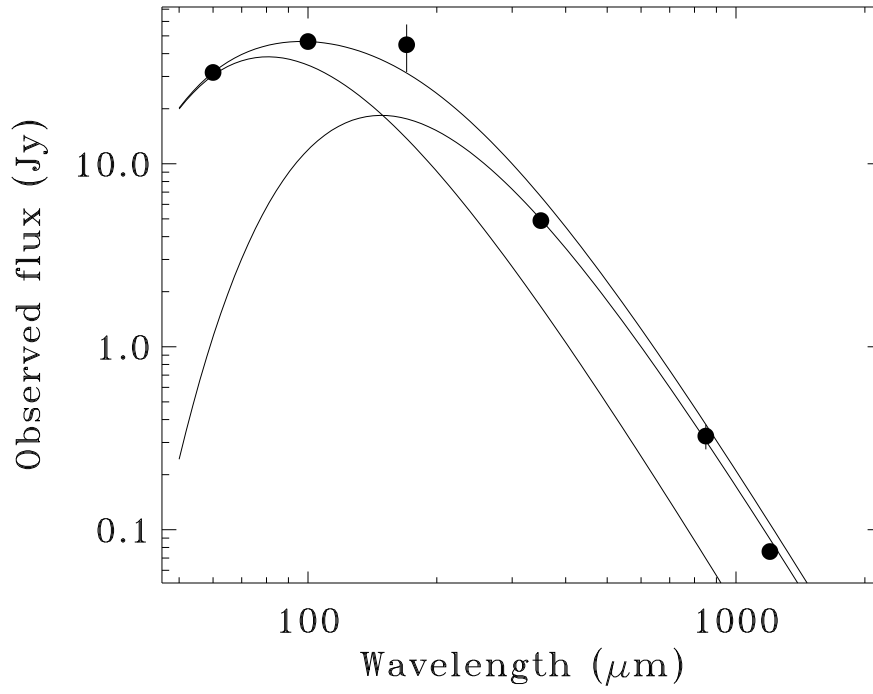
ISOPHOT Serendipity Survey



Local spectral luminosity density



NGC 520



SCUBA Local Universe Galaxy Survey

